






Research Article

Design and Research of Low-Cost and Self-Adaptive Terrestrial Laser Scanning for Indoor Measurement Based on Adaptive Indoor Measurement Scanning Strategy and Structural Characteristics Point Cloud Segmentation

Zhongyue Zhang ¹, Huixing Zhou ^{1,2}, Shun Wang ³, Chongwen Xu ¹,
and Yannan Lv ¹

¹School of Mechanical-Electronic and Vehicle Engineering, Beijing University of Civil Engineering and Architecture, Beijing 100044, China

²Beijing Engineering Research Center of Monitoring for Construction Safety, Beijing 100044, China

³School of Civil and Transportation Engineering, Beijing University of Civil Engineering and Architecture, Beijing 100044, China

Correspondence should be addressed to Huixing Zhou; zhouhuixing@bucea.edu.cn

Received 13 February 2022; Accepted 15 June 2022; Published 21 July 2022

Academic Editor: Jianyong Han

Copyright © 2022 Zhongyue Zhang et al. This is an open access article distributed under the Creative Commons Attribution License, which permits unrestricted use, distribution, and reproduction in any medium, provided the original work is properly cited.

Nowadays, TLS (terrestrial laser scanning) has been a relatively mature measuring equipment categorized to indoor measuring robots, but it is not widely adopted in indoor construction measurement at present. What accounts for its limited application are as follows: (1) the high cost of high-accuracy laser LIDAR and (2) existing TLS equipment does not possess self-adaptation scanning planning and takes no account of efficiency of point cloud processing and consumption of computing power. This paper proposes a novel TLS equipment and a high-efficiency point cloud processing method customized for the novel equipment, with purpose to achieve self-adaption measurement on the basis of indoor characteristics of construction during civil engineering at low cost. This paper mainly presents two parts of innovations: (1) for planning of scanning, the novel TLS features planning sampling density of scanning according to room size and converting scanning data from poses to point clouds, and (2) for processing of point clouds, this paper proposes two novel segmentation algorithms, namely, “on-boundary segmentation algorithm” and “on-angular-distance segmentation algorithm,” based on indoor spatial structure features and characteristics of TLS. Besides, this paper presents modified RANSAC-TLS (random sample consensus-total least squares) plane fitting algorithm, on basis of TLS point cloud distribution characteristics and spatial transformation. Through actual measurement test, it is concluded that the “on-boundary segmentation algorithm” and “on-angular-distance segmentation algorithm” are suitable for point cloud segmentation in different types of scenes. The modified RANSAC-TLS have made a great improvement on accuracy of fitting versus LS (least squares), TLS (total least squares), and RANSAC-LS. Finally, this paper conducts an experiment by executing an actual measurement and then preliminarily testifies the potential and future application of the proposed novel TLS (terrestrial laser scanning) equipment, with measurement parameters from it being changed in the experiment, by comparing with one existing TLS equipment—FARO. The test thus proves the relatively high feasibility and potential of the novel TLS presented in the paper (terrestrial laser scanning) in actual indoor measurement.

1. Introduction

1.1. Background and Meaning. As robot technology and computer technology are advancing speedily, recent years

have seen a certain degree of development in construction robot industry [1, 2]. At construction sites, construction robot replacing manual labour to finish complex work has already become a trending [3–5] such as construction

fabrication robot [6], climbing robot [7], floor-tiling robot [8], collaborative robots [9], and measurement robot [10]. For example, floor-tiling robot [8] completes the automatic floor tiling with high-accuracy robot through control strategy based on visual measurement feedback and finite-state machine. Collaborative robot [9] controlled continuously by a BCI-based system robot to capture workers' brainwaves acquired from a wearable electroencephalogram (EEG) device and interpret them into robotic commands with 90% accuracy. As the feasibility of setting construction robot into practical use in construction process has been enhancing by artificial intelligence and robot technology, the adaptation of computer algorithm and robotics in civil engineering is drawing wider and wider attention among relative science researchers [10–12].

At present, indoor measurement robot is typical of construction robots, and mainstreaming indoor measurement robot is an automatic machine featuring TLS [13, 14]. Differing from traditional manual measurement possesses low-efficiency, high human cost, and high health risk since it needs workers to be exposed to construction environment and to finish work with many tools like guiding rule and feeler gauge [15, 16]. The machine with TLS, which quickly collects 3D information of a room with LIDAR scanning, may be more efficient and be able to attain more comprehensive information of a 3D room.

However, existing equipment with TLS might lead to a waste of work, time, and finance because it is high cost and inevitably produces a tremendous size of point cloud data that usually consumes a large amount of time to process, while the house types and indoor structures of most constructions are actually not complicated and diversified, which means that, in most cases, indoor measurement may not need the possibly excessive collection and processing of information of an indoor room from robot with traditional TLS. Therefore, this paper proposes a self-adaptation TLS system that targets indoor measurement of quantity by combining relevant computer technology and robot technology.

1.2. Related Work

1.2.1. Terrestrial Laser Scanning for Measurement. Terrestrial laser scanning (TLS) is an efficient and reliable method for collecting point clouds, which have a range of applications in the construction. Because of efficient laser scanning data needed in construction, a prior planning optimization process, which can be called planning for scanning (P4S), was used in actual construction project. The key points of the P4S include the type of inputs they assume (model and possible scanning locations), the constraints in measurement, and the algorithm they utilize to solve the optimization problem [17–19]. In terms of algorithm, many researchers have proposed many algorithms to apply in measurement. Nisha Puri [20] presented a compliance-checking algorithm for detecting elements where dimensions exceed specified tolerance, using the synergy of terrestrial laser scanning (TLS) and continuous wavelet

transform (CWT). The results enabled the localization of surface undulations during different characteristic periods. This case displays that the integration of TLS and appropriate algorithm may ensure measurement accuracy. As for indoor measurement and quality assessment, Bosché and Guenet [21] presented an approach that demonstrates the value of this integration for surface flatness control, which employs the Scan-vs-BIM principle of Bosché and e et al. [22] to segment TLS point clouds acquired on-site, by matching each point to the corresponding object in the BIM model. Although it achieves complete and even data analysis during the calculation of flatness of ground, it seems to be of low practicality in real usage because of the requirement for additional processing. Besides, Guo et al. [23] proposed that renting TLS or fractional ownership TLS is more economic for geometric QA, but TLS may be still a high-cost measurement technique.

1.2.2. Advances in Indoor Point Cloud Processing. TLS is mainly used as a data collector, and the data processor is point cloud processing [24–26]. The objective of point cloud processing is to convert 3D information into index for actual measurement, and specific processing technologies include point cloud filtering, point cloud segmentation, and point cloud fitting, among which point cloud segmentation is one research hotspot. In this area, Yin et al. [27] proposed a novel deep learning-based approach, ResPointNet++, by integrating deep residual learning with conventional PointNet++ network. ResPointNet++ shows a high generalizability and remarkable performance, which outperforms conventional PointNet++ by 42% and 23%. Nevertheless, this method for segmentation still requires a relatively large size of dataset for labelling and training. In addition, Park et al. [28] presented a high-performance algorithm to detect discrepancies between an as-planned BIM and the as-is point cloud automatically. The results of experiments showed a significant computation performance improvement: 25.3 and 12.1 times faster than the baseline method for a complex plant facility and a simple indoor building. Although the algorithm shows a relatively large decline in time complexity, a large space complexity sourcing from its fair-sized data determines that it is still difficult for users to remove its dependence on computing power of GPU. Pertinent literature reveals that [29, 30] the key point is to find the proper algorithm of point cloud filtering and point cloud fitting.

1.3. Innovation of This Article. The goal of this paper is to design a low-cost (free from GPU computing power) and adaptive TLS scanning system based on robotics and computer technology. This paper proposes the following innovations:

- (1) We propose a 3D laser scanning structure with two degrees of freedom to realize the self-adaptive scanning with a planning model proposed in this paper, and we realize the conversion of poses from all

laser scanning points into point clouds by the “modified D-H model” in robotics.

- (2) We propose an indoor point cloud process based on scanning data from this TLS, including conditional filtering, two novel point cloud segmentation algorithms, and RANSAC-TLS plane-fitting algorithm based on spatial transformation. In point cloud segmentation processing, this paper not only uses the point cloud but also uses the pose information of the 3D scanning points.

2. Low-Cost and Adaptive Indoor Measurement TLS System

This paper proposes a low-cost and self-adaptive TLS system blending robot technology and computer software technology (see Figure 1). It contains 5 links that integrated well: user level, system layer, drive layer, execution layer, and data layer. The user layer, where user operates the whole machine and reads measuring results, manages human-machine interaction; the system layer performs the master control of motion control, data reading, and transfer of the TLS system; the drive layer is where the system implements servo control; the execution layer regulates motion of servo motor and reads laser ranging data and pose of laser module during a specific task; in data layer, measurement data are transferred from the TLS system to data cloud through a 5G module, by which it is also downloaded to a computer to implement following data processing; and finally, the processed data, transferred to the system layer through the 5G module, turns to be displayed on the user layer at the end.

3. Adaptive Indoor Measurement Scanning Strategy

3.1. Indoor Quantity Measurement Process Analysis. The main objective of an indoor measurement project is to obtain and process the indoor construction quantity information. In traditional manual measurement method, the flatness and verticality degree of indoor are read with walls, which are obtained by traditional manual measurement through the gap between the guiding rule and the feeler gauge. Through the analysis of the principle of the measured quantity engineering, the measured quantity engineering can be transformed into a process of indoor digital information processing.

- (1) Obtaining the comprehensive three-dimensional information of a room with the indoor scanning equipment.
- (2) Classifying the data.
- (3) Processing the classified data and categorizing them into indexes of quantities.

3.2. Adaptive Measurement Scanning Strategy

3.2.1. Scanning Motion Mechanism of Novel TLS in This Paper. The whole laser scanning process is generated by the

motion of a two-degree-of-freedom motor platform. In this paper, a motion mode of “equal angle” is proposed: in a fixed range of motion, we rotate according to the equal angle interval and stay at this position for distance measurement with laser module. The novel TLS will automatically scan the entire room by repeating the motion mode of “equal-angle” several times. The scanning motion of the novel TLS is based on a two-degree-of-freedom motor platform, with a “horizontal-motion motor” and a “vertical-motion motor.” In order to complete the indoor laser scanning more efficiently, the laser module has multilasers in the equal angle distribution (see Figure 2) (more details about the novel TLS equipment can be watched in a video by clicking on the link <https://youtu.be/h7SavWCaPvc>).

The entire scanning process comprises many such motor-motion cycles (see Figure 3). The “vertical pitching-motion motor” finishes one “equal-angle” (not greater than 360 degree) rotation, with the “horizontal spinning-motion motor” keeping static and repeating rotations in the same pattern many times, and the laser scanning will have a whole-room coverage.

In order to achieve self-adaptation planning for scanning, namely, self-P4S (planning for scanning), with a certain scanning density preset by operators in specific measuring projects for different-size rooms, the novel TLS fulfils to finish scanning in shortest time.

3.2.2. Maximum Distance Interval Scanning in Planning Model. The distribution of point cloud under multiprocess scanning is irregularity. In order to plan the scanning density of indoor-scanning point cloud, we propose the maximum distance interval of point cloud in the planning model “ s_0 ,” which is the distance between scanning paths of the largest plane in the hexahedral room (see Figure 4). Referring to the ACI standard [31], we define the maximum standard $s_{\max} = 330$ mm, and the relationship between s_0 and s_{\max} is as follows:

$$s_0 \leq s_{\max}. \quad (1)$$

3.2.3. Minimum Time Cost Programming Model. In actual measurement, not only the density of point cloud but also the efficiency of measurement should be considered. Therefore, this paper proposes the “minimum time cost programming model.”

The model takes the minimum time consumption as the objective and the minimum distance interval of scanning as the constraint condition. The specific formula is as follows:

$$T_A = n_A \times T_s + T_y = \min. \quad (2)$$

In the objective function, n_A represents the total number of times the laser module has been executed by the device during the movement. T_A represents the overall elapsed time for the device to perform an indoor 3D scanning. T_s represents the time spent by the laser module in a single scanning. T_y represents the total elapsed time of the device during the movement. The constraints of the objective function are expressed as follows:

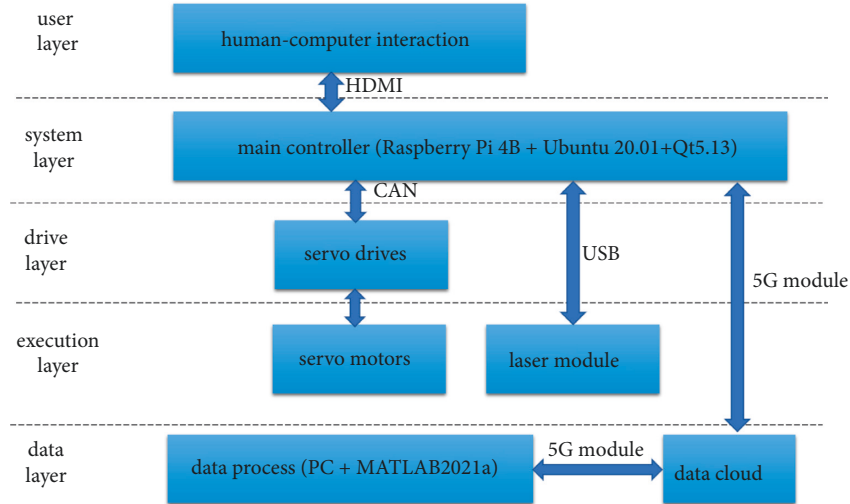
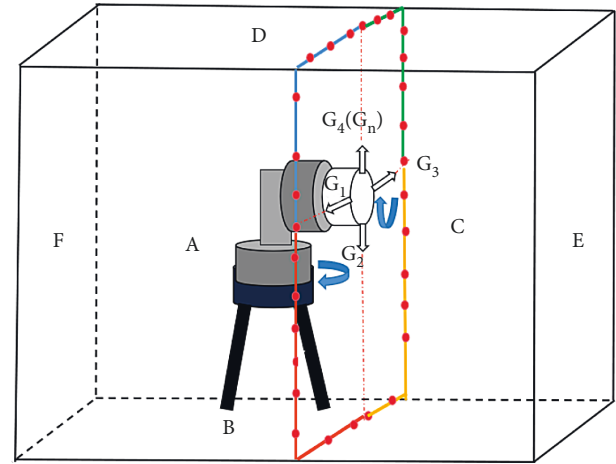


FIGURE 1: The frame of the self-adaptive TLS system.

$$\left\{ \begin{array}{l} n_1 = \frac{\theta_{1A}}{\Delta\theta_1}, \\ n_2 = \frac{\theta_{2A}}{\Delta\theta_2}, \\ n_A = n_1 \times n_2, \\ T_y = (n_A - 1) \times T_d, \\ s_m \leq s_0, \\ \Delta\theta_2 = k\Delta\theta_1, \\ \Delta\theta_1 = \text{ROUND}(\theta_c). \end{array} \right. \quad (3)$$

θ_{1A} represents the total range of motor rotation angles in a single pass of the horizontal motor. θ_{2A} represents the total range of motor rotation angles in a single pass of the pitch motor. $\Delta\theta_1$ and $\Delta\theta_2$ represent the angular interval values of



Range of Laser 1: —
 Range of Laser 2: —
 Range of Laser 3: —
 Range of Laser 4: —

FIGURE 2: The diagram of scanning with the laser module.

the “equal angle” motion of the horizontal motor and the elevation motor, respectively, in a single process. θ_c (shown in Figure 5) is calculated as follows:

$$\theta_c = \arccos\left(\frac{L_c^2 + L_b^2 + 2s_0L_b}{4\sqrt{(L_b/2)^2 + (L_c/2)^2}\sqrt{(L_b/2 - s_0)^2 + (L_c/2)^2}}\right) + \arccos\left(\frac{D_0}{\sqrt{(L_b/2)^2 + (L_c/2)^2}}\right) - \arccos\left(\frac{D_0}{\sqrt{(L_b/2 - s_0)^2 + (L_c/2)^2}}\right). \quad (4)$$

In the above formula, L_a , L_b , and L_c , respectively, represent interior net story height, length of longer wall, and length of shorter wall.

3.3. Converting from Scanning Data to Point Cloud Data. Some parameters may be obtained from the novel absolute angles of the “horizontal spinning-motion motor” and the

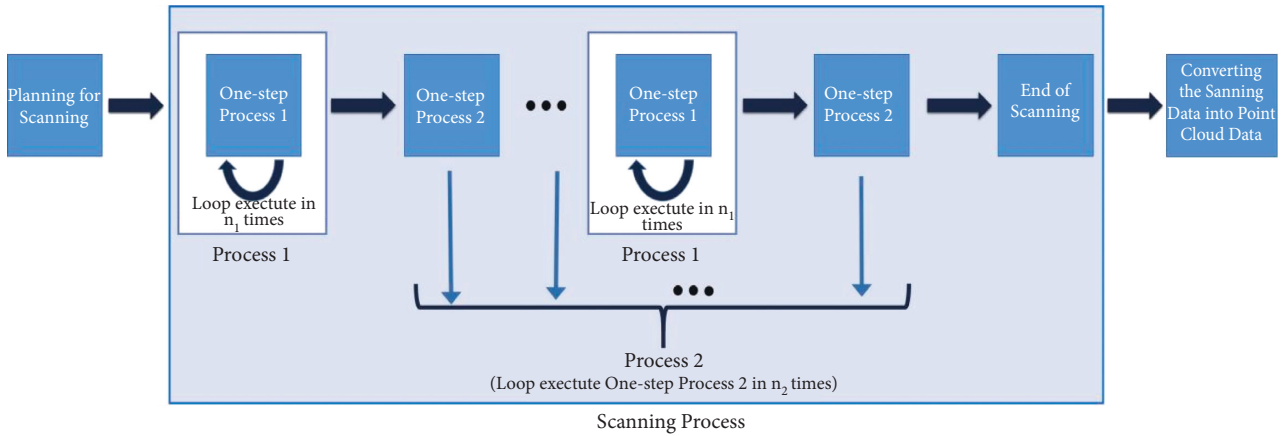
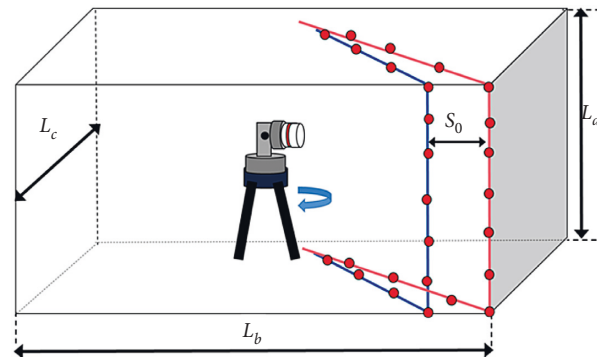


FIGURE 3: The flow chart of the indoor scanning process.



Comments table

- Center of TLS
- Laser point
- The farthest path of laser scanning
- The second farthest path of laser scanning
- ▭ The room

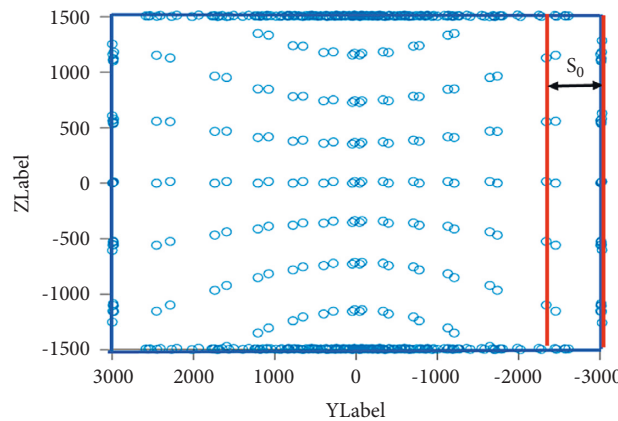
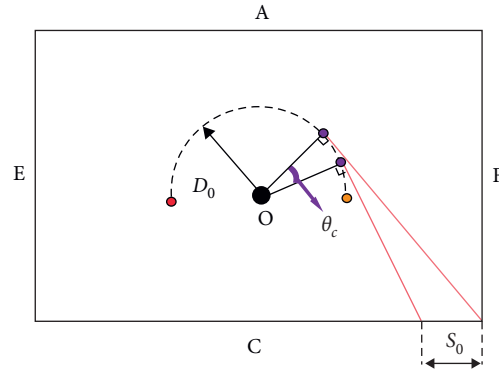


FIGURE 4: The calculation diagram of the maximum distance interval.

“vertical pitching-motion motor.” The poses of laser scanning points (the TLS machine as the origin in the coordinate system) can be attained on these parameters. In order to convert poses of laser scanning points into point clouds, this paper makes use of “modified DH modelling” in robotics and realizes it in this way.

The following is an illustration of the converting process of the data from one single laser scanning point. Based on the novel TLS equipment and “modified DH modelling,” this paper builds four coordinate systems marked as {0}, {1}, {2}, and {3}. The origin of {0} system is the intersection point of medial axis of the horizontal motor and the



Comments table

- Center of TLS
- Start of laser module motion path
- End of laser module motion path
- Offset point
- ⋯ Motion path of laser module
- Path of laser
- The room overlooking

FIGURE 5: The scanning model analysis diagram.

medial axis of the vertical motor; the origin of {1}, with the horizontal spinning-motion motor as its origin, represents a coordinate system overlapped with {0}; {2} is the coordinate system with the vertical pitching-motion motor as its origin; and {3} is established with the single laser scanning point as its origin. In modified D-H method, the coordinate frame i is attached to the near (proximal) end of link i as shown in Figure 6. The link and joint parameters are defined as D-H parameters and are summarized in Table 1.

In practice, because measuring with single-laser laser module is not efficient enough, this paper presents a laser module with four lasers. The four lasers array around the

centre of the laser module, which is coaxial with the vertical pitching-motion motor, with an angular distance of 90 degree between every two of them. Such laser module may be referred as multi-laser-ranging module.

As for all lasers in the laser module, the link and joint parameters are defined as D-H parameters and are summarize in Table 1. In the table, θ_i represents the angular separation of laser i from the initial laser. L_i represents the measured value of laser i .

The link transformation from frame {0} to frame {3} can be written as follows:

$${}^3_0T_i = \begin{bmatrix} \cos \theta_1 \cos (\theta_2 + \theta_i) & -\cos \theta_1 \sin (\theta_2 + \theta_i) & \sin \theta_1 & D_0 \sin \theta_1 + D_1 \cos \theta_1 \cos (\theta_2 + \theta_i) \\ \sin \theta_1 \cos \theta_2 & -\sin \theta_1 \sin (\theta_2 + \theta_i) & -\cos \theta_1 & D_1 \cos \theta_1 \sin \theta_1 - D_0 \cos \theta_1 \\ \sin (\theta_2 + \theta_i) & \cos (\theta_2 + \theta_i) & 0 & D_1 \sin (\theta_2 + \theta_i) \\ 0 & 0 & 0 & 1 \end{bmatrix}. \quad (5)$$

The three-dimensional coordinates of the laser point are as follows:

$$\begin{cases} p_{xi} = D_0 \sin \theta_1 + D_1 \cos \theta_1 \cos (\theta_2 + \theta_i), \\ p_{yi} = D_1 \cos \theta_1 \sin \theta_1 - D_0 \cos \theta_1, \\ p_{zi} = D_1 \sin (\theta_2 + \theta_i). \end{cases} \quad (6)$$

4. Indoor Point Cloud Process

4.1. Overview of Point Cloud Processing Procedures. According to text above, 3D point clouds and poses of 3D point clouds are presented by converting laser scanning data through

modified DH modelling. Next, the novel TLS will enter phase of point cloud processing. As shown in the flow chart (see Figure 7), the data obtained from previous scanning activity will go through point cloud processing, including point cloud filtering, point cloud segmentation, and point cloud fitting. Experiencing the three procedures of processing, the processed point cloud data can be directly used to calculate quantities of the measured construction since every interior surface of the construction can be represented by a mathematical equation.

4.2. Indoor Conditional Point Cloud Filtering. Because refraction occurs when laser beam hits on glasses and it will cause the laser ranging value to be greater than the actual

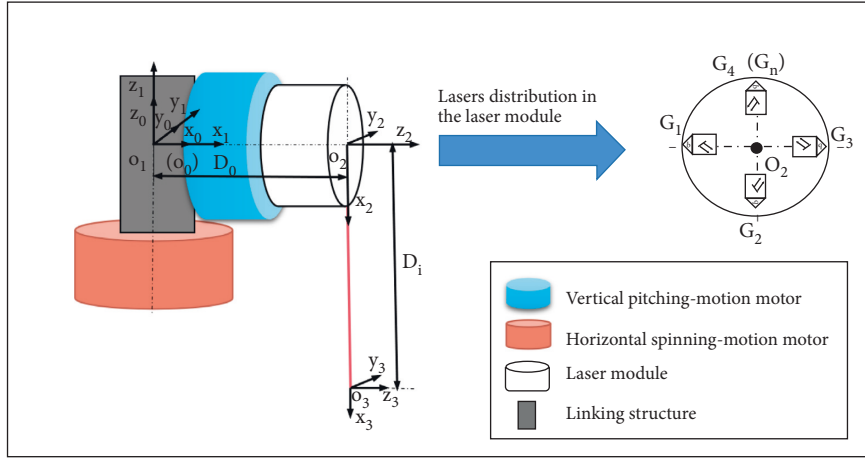


FIGURE 6: The modified D-H model analysis diagram of the TLS.

TABLE 1: Parameters of modified D-H method for all lasers.

Aix	Link length $a_{(i-1)}$	Link twist $\alpha_{(i-1)}$	Joint offsite b_i	Joint angle θ_i
{1}	0	0°	0	θ_1
{2}	0	90°	D_0	$\theta_1 + \theta_i$
{3}	D_i	0°	0	0°



FIGURE 7: The flow chart of the indoor point cloud process.

value, point clouds extracted around door and window may usually present abnormality in practical measuring. Abnormal point clouds need to be eliminated during point cloud processing.

This paper utilizes conditional point cloud filter and distributing characteristics of indoor point clouds to identify abnormal point clouds. Indoor point clouds roughly distribute in form similar to hexahedron, and the centre of TLS equipment is basically located at the centre of measuring room. This paper defines the distance between the centre of the TLS equipment and the farthest point relative to the centre of the TLS equipment as “maximum polar radius”; in this situation, distance from every point cloud to the centre of the equipment is not supposed to surpass the “maximum polar radius”; and any point cloud not in conformity with the criterion above should be identified as an abnormal point cloud.

It is known that L_a , L_b , and L_c , respectively, represent interior net story height, length of longer wall, and length of shorter wall; the “maximum polar radius” of room is r_t ; the distance from any point cloud (x_i, y_i, z_i) to the centre of the novel TLS equipment is marked as r_i ; r_t and r_i can be expressed as follows:

$$\begin{cases} r_t = \sqrt{(\beta_1 r_a)^2 + (\beta_2 r_b)^2 + (\beta_3 r_c)^2}, \\ r_i = \sqrt{(x_i)^2 + (y_i)^2 + (z_i)^2}. \end{cases} \quad (7)$$

In the formula above, β_1 , β_2 , and β_3 are correction factors within the range (1, 1.5). The correction factor is of significance since only under ideal condition, the centre of the novel TLS equipment may be located just at the centre of a room.

4.3. Segmentation of Indoor Point Clouds Based on Structural Characteristic. Segmentation of point clouds is a core procedure of data processing, and this paper proposes two algorithms for segmenting point clouds based on structural characteristics. Namely, this paper makes full use of point clouds and poses of them and spatial geometric features of room to create two novel algorithms.

4.3.1. On-Boundary Segmentation Algorithm for Indoor Point Cloud. In this paper, point clouds extracted from the novel self-adaptive TLS equipment present following features: 1. in each “process one,” the angle distance between the original point cloud and the final point cloud from the same single laser will present 90 degree. 2. Similarly, in one “process two,” the angle separation between the original point cloud and the final point cloud from a single laser is sure to be 180 degree. 3. Point clouds distribute in a form similar to a hexahedron. 4. Original state of the novel TLS equipment is with four lasers in the laser module separately vertical to four different interior surfaces, and the centre of the equipment is put close to the centre of the room.

This paper names this novel segmentation algorithm as “on-boundary segmentation for indoor point cloud,” and the whole process is consisted of two rounds of segmentation. The first round is segmenting out the ceiling and floor, and the second round is segmenting out four interior walls of measured room (see Figure 8).

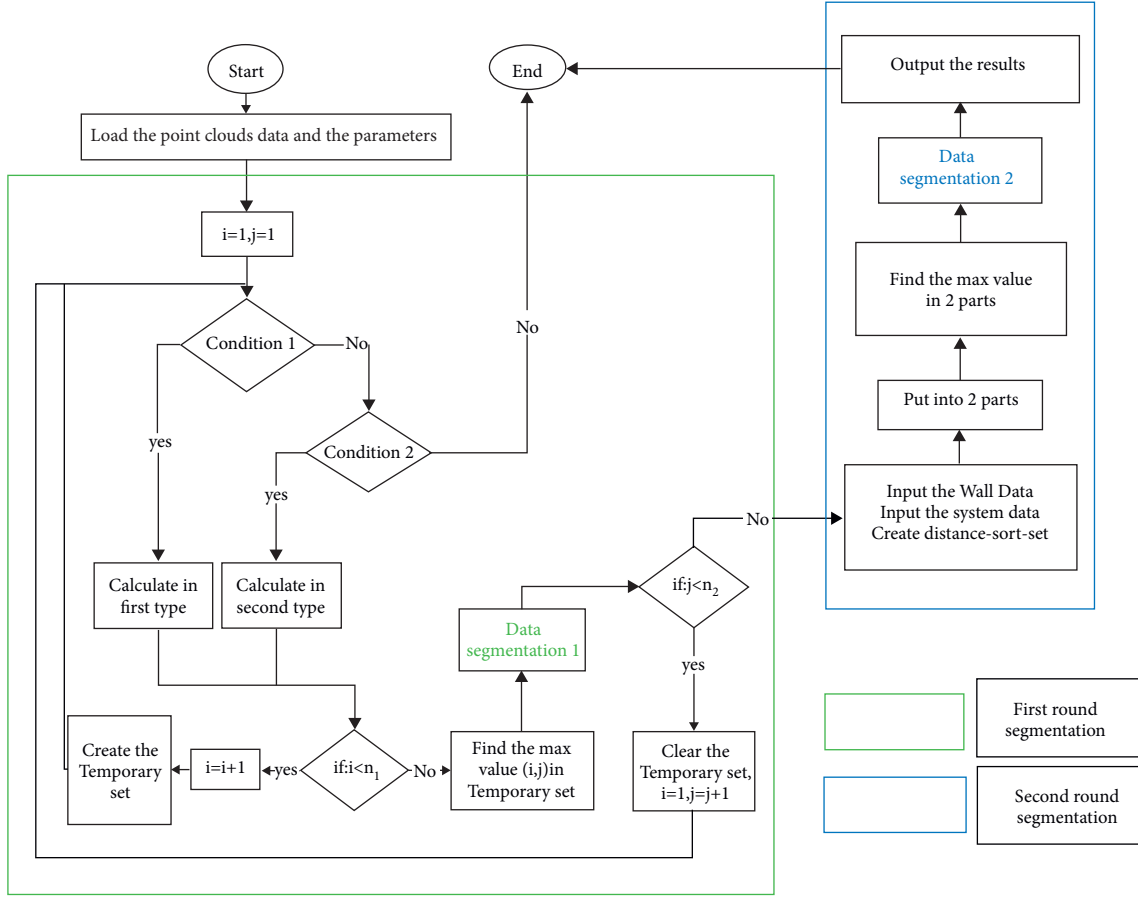


FIGURE 8: The flow chart of on-boundary segmentation algorithm.

(1) *First Round of Segmentation.* Here, only one laser L_i is taken to illustrate distributing characteristics and dataset of point clouds from one single laser after the whole scanning process. When the entire scanning phase of measurement is over, it is manifested that all point clouds extracted from laser L_i are placed on $Wall_{Data(i)}$, $Wall_{Data(i+1)}$, $Wall_{Data(i+2)}$, and a plane (ceiling or floor). All point clouds from laser L_i form a point cloud dataset $\{P_{L_i,j}\}$, in which the “ L_i ” represents point clouds from the laser, and “ i ” and “ j ” represent, respectively, the first-conducted “one-step process one” in first “process one” and first-conducted “one-step process two” in first “process two.” In addition, it is known that single “process one” contains n_1 times of “one-step process one” and single “process two” contains n_2 times of “one-step process two.”

With the point cloud dataset, distributing characteristics explained above and the concept “offset point” mentioned before, the following will demonstrate the first round of segmentation in detail. Firstly, all the point cloud data from first “one-step process two” gather into a dataset $\{P_{L_i,1}\}$, and data in it may be present as $\{P_{L_i,11}, P_{L_i,21}, P_{L_i,31} \dots P_{L_i,n_1,1}\}$. The coordinates of every $P_{L_i,1}$ may be marked as $(x_{L_i,1}, y_{L_i,1}, z_{L_i,1})$. In that, the borderline segmentation algorithm requires the distance from point clouds to the “offset point” to identify the boundary of surfaces, and the coordinates of the “offset point” need to be used in calculation (see Figure 9). As for the coordinates of “the offset point” $O_{p_{L_i,j}}$ this paper has to acquire them by classified discussion and the formula is as follows:

$$\begin{cases} x_{p_{L_i,j}} = \sin(\Delta\theta_2 j)D_0, y_{p_{L_i,j}} = -\cos(\Delta\theta_2 j)D_0, z_{p_{L_i,j}} = 0, & \left(0 < \Delta\theta_2 j < \frac{\pi}{2}\right), \\ x_{p_{L_i,j}} = \cos\left(\Delta\theta_2 j - \frac{\pi}{2}\right)D_0, y_{p_{L_i,j}} = \sin\left(\Delta\theta_2 j - \frac{\pi}{2}\right)D_0, z_{p_{L_i,j}} = 0, & \left(\frac{\pi}{2} < \Delta\theta_2 j < \pi\right). \end{cases} \quad (8)$$

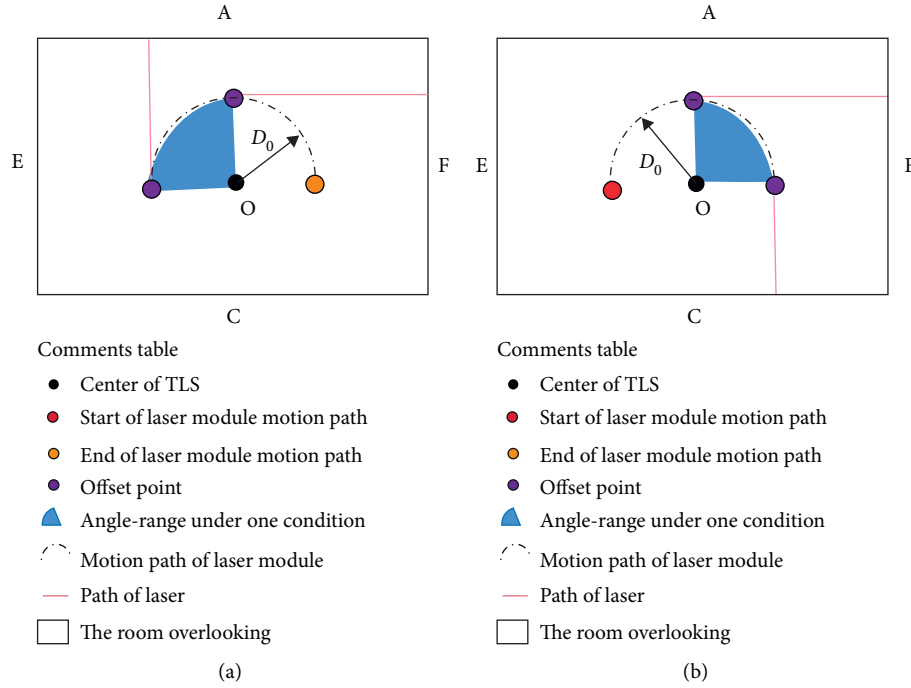


FIGURE 9: Offset point in laser scanning. (a) Condition 1. (b) Condition 2.

The equation represents the distance between every point cloud and the offset point, which is as follows:

$$P_{L_i i1 d} = \sqrt{(x_{L_i i1} - x_{pL_i ij})^2 + (y_{L_i i1} - y_{pL_i ij})^2 + (z_{L_i i1} - z_{pL_i ij})^2}. \quad (9)$$

Next, this paper identify the maximum value of the dataset $\{P_{L_i i1 d}\}$:

$$P_{L_i i1 d_{max}} = \max\{P_{L_i 11 d}, P_{L_i 21 d}, P_{L_i 31 d} \dots P_{L_i n_1 1 d}\}. \quad (10)$$

This paper puts serial numbers on every point clouds in sequence according to clockwise direction, and the

$P_{L_i i1 d_{max}} = \max\{P_{L_i 11 d}, P_{L_i 21 d}, P_{L_i 31 d} \dots P_{L_i n_1 1 d}\}$ is numbered as $L_i i1_{max}$. The $L_i i1_{max}$ can be the dividing point of this set of point clouds so that all the point clouds can be separated into ceiling surface or wall surface, and they may be present as follows:

$$\begin{aligned} \text{Plane}_{\text{Data}} &= \{P_{L_i i_{max} 1}, P_{L_i (i_{max}+1) 1}, P_{L_i (i_{max}+2) 1} \dots P_{L_i n_1 1}\}, \\ \text{Wall}_{\text{Data}} &= \{P_{L_i 11}, P_{L_i 21}, P_{L_i 31} \dots P_{L_i (i_{max}-1) 1}\}. \end{aligned} \quad (11)$$

The end of the entire set of procedures in the first round of segmentation signifies that the segmentation of point clouds from laser L_i in a “one-step process one” is over. When the set of procedures is repeatedly executed n_2 times with n_2 sets of point clouds to be put into the algorithm, all point clouds of laser L_i that are obtained from the entire scanning process and that are also distributed on ceiling or floor surfaces will be segmented out from other point cloud clusters.

(2) *The Second Round of Segmentation.* Points clouds from laser L_i on ceiling and floor are segmented out through the first round of segmentation, but those on three walls are left for segmenting. However, there are also edges between every two walls, and the borderline segmentation method is also applicable to segmenting point clouds from laser L_i on four walls, which are ready to be put into three dataset marked as $\text{Wall}_{\text{Data}i}$, $\text{Wall}_{\text{Data}(i+1)}$, and $\text{Wall}_{\text{Data}(i+2)}$. During the first round of segmentation of point clouds from laser L_i , in one

“process one,” all point clouds not in dataset of ceiling or floor are retained in the form of an array and all point clouds are present in dataset $\{\{P_{L_i ij}\}\}_{m \times n_2}$ (m is the maximum number in one case process one in first round of segmentation).

$$\{\{P_{L_i ij}\}\}_{m \times n_2} = \{\{P_{L_i i1}\}_{m \times 1}, \{P_{L_i i2}\}_{m \times 1}, \{P_{L_i i3}\}_{m \times 1}, \dots, \{P_{L_i in_2}\}_{m \times 1}\}. \quad (12)$$

This paper selects point clouds numbered as the first one in every array to form a point cloud dataset $\{P_{L_i 1j}\}_t$ for tagging, which will be used to identify the “tagging point on edges” (the point cloud nearest to the cross-point of the horizontal cross-lines and edges of two adjacent walls) (see Figure 10).

$$\{P_{L_i 1j}\}_t = \{P_{L_i 11}, P_{L_i 12}, P_{L_i 13} \dots P_{L_i 1n_2}\}. \quad (13)$$

Since there are two “tagging points on edges” in the point cloud set for tagging, this paper divides the whole dataset into two parts, $\{P_{L_i 1m}\}$ and $\{P_{L_i 1n}\}$.

$$\begin{aligned} \{P_{L_i 1m}\} &= \{P_{L_i 11}, P_{L_i 12}, P_{L_i 13} \dots P_{L_i 1(n_2/2)}\}, \\ \{P_{L_i 1n}\} &= \{P_{L_i 1((n_2/2)+1)}, P_{L_i 12}, P_{L_i 13} \dots P_{L_i 1n_2}\}. \end{aligned} \quad (14)$$

Actually, the two tagging points on edges are separately in the two datasets $\{P_{L_i 1m}\}$ and $\{P_{L_i 1n}\}$, and they are two point clouds that, respectively, have longest distance to the centre of the equipment in their dataset. The formulae of them are as follows:

$$\begin{aligned} P_{L_i 1md} &= \sqrt{(x_{11m})^2 + (y_{11m})^2 + (z_{11m})^2}, \\ P_{L_i 1nd} &= \sqrt{(x_{L_i 1n})^2 + (y_{L_i 1n})^2 + (z_{L_i 1n})^2}. \end{aligned} \quad (15)$$

Identifying the two “tagging points on edges” is as follows:

$$\begin{aligned} P_{L_i 1md_{\max}} &= \max \{P_{L_i 11d}, P_{L_i 12d}, P_{L_i 13d} \dots P_{L_i 1(n_2/2)d}\}, \\ P_{L_i 1nd_{\max}} &= \max \{P_{L_i 1((n_2/2)+1)d}, P_{L_i 1((n_2/2)+2)d}, P_{L_i 1((n_2/2)+3)d} \dots P_{L_i 1n_2d}\}. \end{aligned} \quad (16)$$

From this, the number of the two tagging points is obtained and they serve as dividing points to segment point

clouds separately into three walls $\text{Wall}_{\text{Data}i}$, $\text{Wall}_{\text{Data}(i+1)}$, and $\text{Wall}_{\text{Data}(i+2)}$.

$$\begin{aligned} \text{Wall}_{\text{Data}i} &= \{\{P_{1i1}\}, \{P_{1i2}\}, \{P_{1i3}\}, \dots, \{P_{1im_{\max}}\}\}, \\ \text{Wall}_{\text{Data}(i+1)} &= \{\{P_{1i(m_{\max}+1)}\}, \{P_{1i(m_{\max}+2)}\}, \{P_{1i(m_{\max}+3)}\}, \dots, \{P_{1in_{\max}}\}\}, \\ \text{Wall}_{\text{Data}(i+2)} &= \{\{P_{1i(n_{\max}+1)}\}, \{P_{1i(n_{\max}+2)}\}, \{P_{1i(n_{\max}+3)}\}, \dots, \{P_{1in_2}\}\}. \end{aligned} \quad (17)$$

After implementing the first and second rounds, the segmentation processing for all points clouds extracted from entire scanning of laser L_i comes to its end and all point cloud data are segmented into four datasets $\text{Plane}_{\text{Data}}$, $\text{Wall}_{\text{Data}i}$, $\text{Wall}_{\text{Data}(i+1)}$, and $\text{Wall}_{\text{Data}(i+2)}$.

When point clouds collected from all the four laser modules have finished the first and second rounds of segmentation algorithm processing, the results of segmentation of point clouds on all interior surfaces will be attained.

4.3.2. On-Angular-Distance Segmentation Algorithm for Indoor Point Cloud. Apart from the novel segmentation algorithm introduced above, this paper proposes a novel segmentation algorithm for indoor point clouds based on angular distance emerging during scanning process (Figure 11). The laser beam from laser L_i will hit on some points in the intersection line of two wall surfaces when the laser module on

vertical pitching-motion motor moves in circle along with the horizontal spinning-motion motor. At the moment, an angular distance presents between two lines, one from current position of laser module to the centre of the equipment and another from original position of laser module to the centre. This angular distance is marked as $\theta_{w_i w_{(i+1)}}$, which is called “wall-to-wall angular distance” in this paper, and $\theta_{w_{(i+1)} w_{(i+2)}}$ is another “wall-to-wall angular distance.” (Figures 12(a) and 12(d)). $\theta_{(w_i p)_j}$ represents an angular separation occurs when the laser beam from L_i hits on the intersection line of wall and ceiling or floor, and one line starts from the intersection line to the spatial position of the laser module and another line from it to the centre of the TLS machine. $\theta_{(w_i p)_j}$ is named to be “wall-to-plane angle” (Figure 13), and the “ j ” means the times of conducting “process two.” However, accompanying implementation of all times of “process two,” there are four different formulae for calculating “wall to plane angle” in correspondence to four range of angular distance.

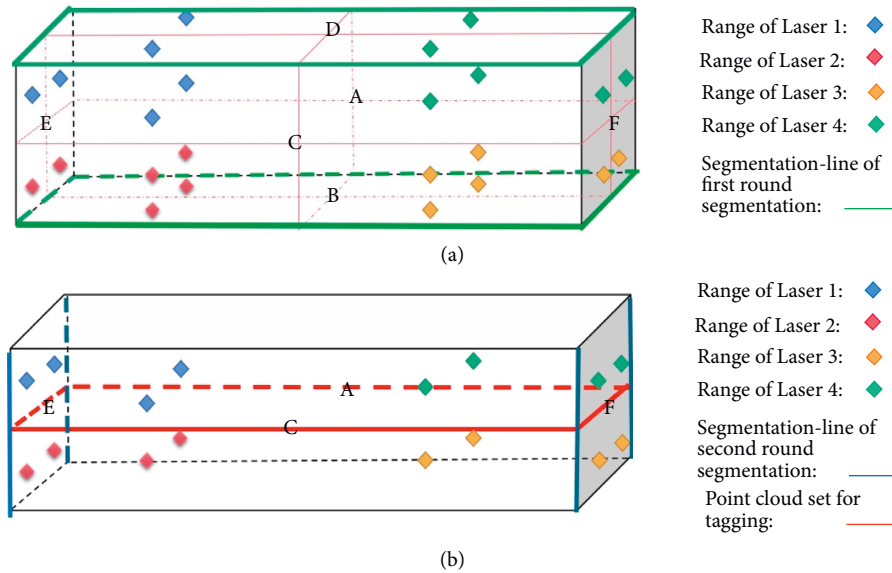


FIGURE 10: The diagram of on-boundary segmentation algorithm. (a) First-round segmentation. (b) Second-round segmentation.

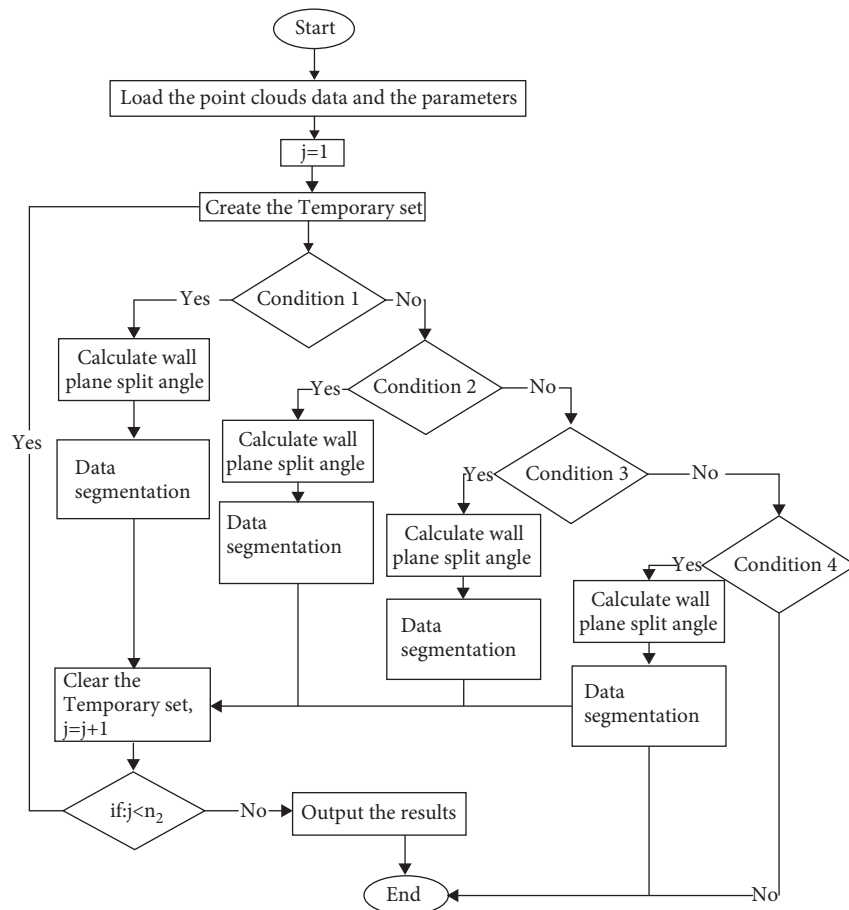


FIGURE 11: The flow chart of the on-angular-distance segmentation algorithm.

(1) *Procedures of Segmentation Algorithm on Angle Characteristics.* This segmentation algorithm on angle characteristics needs information, apart from point clouds, including interior net story height and the length of long and

short wall of room. With this information, the procedures of segmentation algorithm on angle characteristics for point clouds collected from a single laser are demonstrated in Figure 12. As shown in Figure 12, after obtaining “wall-to-

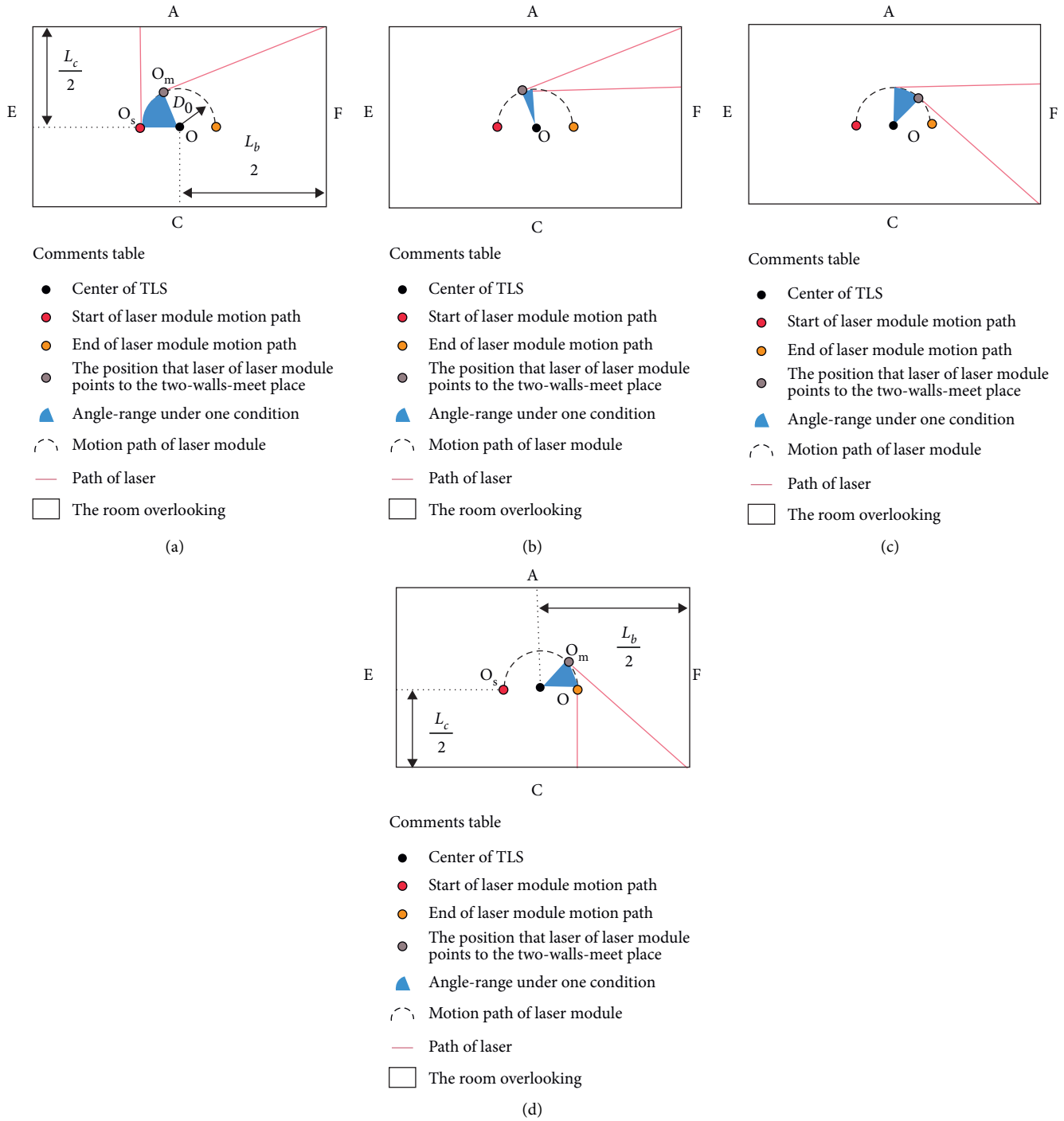


FIGURE 12: The diagram of “wall-to-wall angle” and different conditions ($\angle O_s O O_m$ in (a), (d) is the “wall-to-wall angle”). (a) Condition 1. (b) Condition 2. (c) Condition 3. (d) Condition 4.

“wall” or “wall-to-plane” angles, the algorithm processes point clouds in different formulae in accordance with which range the $j\Delta\theta_2$ is divided into.

The procedures of algorithm processing are shown in Figure 11. Firstly, the point clouds and parameters of room size are loaded and the system will calculate the “wall-to-wall angle” and “plane-to-wall angle” on the given parameters. Then, it enters the branch structure to judge which formula to be

invoked based on angular ranges of $j\Delta\theta_2$. When the branch structure is terminated, point clouds extracted from one single laser L_i during the entire scanning process will be segmented into four datasets, respectively, relative to four interior surfaces: $Plane_{Data}$, $Wall_{Data_i}$, $Wall_{Data(i+1)}$, and $Wall_{Data(i+2)}$.

(2) *The Calculation of “Wall-to-Wall Angle.”* Here, only a single laser L_i is taken as a sample to calculate “wall-to-wall

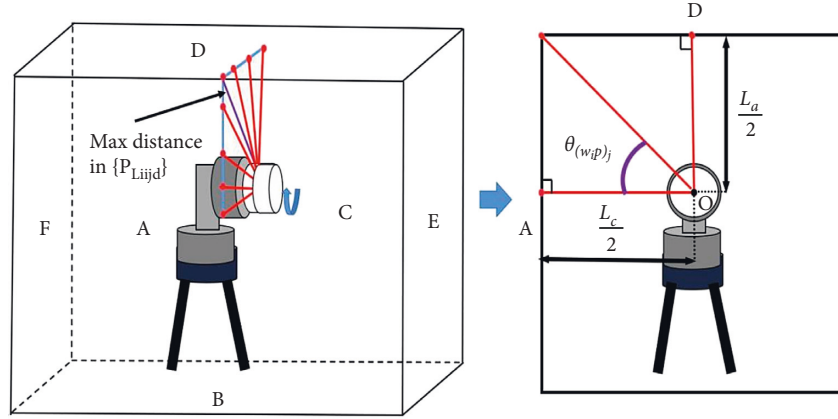


FIGURE 13: The diagram of point cloud segmentation in scanning of “process one.”

angle.” As shown in Figures 12(a) and 12(d), this paper may calculate the angle $\theta_{w_i w_{(i+1)}}$ and $\theta_{w_{(i+1)} w_{(i+2)}}$ with given interior net story height and length of walls in the following formula:

$$\theta_{w_i w_{(i+1)}} = \frac{\pi}{2} + \arccos\left(\frac{\sqrt{(L_b/2)^2 + (L_c/2)^2}}{\sqrt{(L_b/2)^2 + (L_c/2)^2 - D_0^2}}\right) - \arctan\left(\frac{L_c}{L_b}\right), \quad (18)$$

$$\theta_{w_{(i+1)} w_{(i+2)}} = \pi + \arccos\left(\frac{\sqrt{(L_b/2)^2 + (L_c/2)^2}}{\sqrt{(L_b/2)^2 + (L_c/2)^2 - D_0^2}}\right) - \arctan\left(\frac{L_b}{L_c}\right).$$

(3) *The Calculation of “Wall-to-Plane Angle.”* With loaded point cloud data and parameters of room size, the variable range of $j\Delta\theta_2$ determines different formulae to calculate the “wall-to-plane angle,” which is relative to the position of the

“horizontal spinning-motion motor” as the angular distance of it and its original position is equal to $j\Delta\theta_2$. All four different formulae for calculating “wall-to-plane angle” (see Figures 12 and 13), also “ $\theta_{(w,p)_j}$,” are as follows:

$$\left\{ \begin{array}{l} \theta_{(w,p)_j} = \arctan\left(\frac{L_a \cos(j\Delta\theta_2)}{2((L_c/2) - \sin(j\Delta\theta_2)D_0)}\right), \quad (0 < \Delta\theta_2 j < \Delta\theta_{w_i w_{(i+1)}}), \\ \theta_{(w,p)_j} = \arctan\left(\frac{L_a \sin(j\Delta\theta_2)}{2((L_b/2) + \cos(j\Delta\theta_2)D_0)}\right), \quad (\Delta\theta_{w_i w_{(i+1)}} < \Delta\theta_2 j < \frac{\pi}{2}), \\ \theta_{(w,p)_j} = \arctan\left(\frac{L_a \cos(j\Delta\theta_2 - (\pi/2))}{2((L_b/2) - \sin(j\Delta\theta_2 - (\pi/2))D_0)}\right), \quad (\frac{\pi}{2} < \Delta\theta_2 j < \Delta\theta_{w_{(i+1)} w_{(i+2)}}), \\ \theta_{(w,p)_j} = \arctan\left(\frac{L_a \cos(\pi - j\Delta\theta_2)}{2((L_c/2) + \sin(\pi - j\Delta\theta_2)D_0)}\right), \quad (\Delta\theta_{w_{(i+1)} w_{(i+2)}} < \Delta\theta_2 j < \pi). \end{array} \right. \quad (19)$$

(4) *Procedures of Data Segmentation.* As known above, accompanying $j\Delta\theta_2$ within different range, the calculation formula to get one certain degree value $\theta_{(w,p)_j}$ diverges and so does the segmentation results of relevant point clouds. Here, it comes a i_{θ_1} to help in segmenting point clouds into different datasets, and its equation is $i_{\theta_1} = \theta_{(w,p)_j} / \Delta\theta_1$.

All the point clouds are loaded in a dataset $\{\{P_{L_{ij}}\}\}_{n_1 \times n_2}$, and it is comprised of many datasets. $\{P_{L_{ij}}\}_{n_1 \times 1}$ is the only object to be processed in loop structure

$$\{\{P_{L_{ij}}\}\}_{n_1 \times n_2} = \left\{ \{P_{L_{i1}}\}_{n_1 \times 1}, \{P_{L_{i2}}\}_{n_1 \times 1}, \{P_{L_{i3}}\}_{n_1 \times 1}, \dots, \{P_{L_{im_2}}\}_{n_1 \times 1} \right\}. \quad (20)$$

If for $j\Delta\theta_2$, $0 < j\Delta\theta_2 < \Delta\theta_{w_i w_{(i+1)}}$:

$$\text{Plane}_{\text{Data}} = \left\{ P_{L_{i_{\theta_1} j}}, P_{L_{(i_{\theta_1}+1)j}}, P_{L_{(i_{\theta_1}+2)j}}, \dots, P_{L_{i_{m_1} j}} \right\}, \quad (21)$$

$$\text{Wall}_{\text{Data}i} = \left\{ P_{L_{i1j}}, P_{L_{i2j}}, P_{L_{i3j}}, \dots, P_{L_{(i_{\theta_1}-1)j}} \right\}.$$

If for $j\Delta\theta_2$, $\Delta\theta_{w_i w_{(i+1)}} < \Delta\theta_2 j < \pi/2$:

$$\text{Plane}_{\text{Data}} = \left\{ P_{L_{i_{\theta_1} j}}, P_{L_{(i_{\theta_1}+1)j}}, P_{L_{(i_{\theta_1}+2)j}}, \dots, P_{L_{i_{m_1} j}} \right\},$$

$$\text{Wall}_{\text{Data}(i+1)} = \left\{ P_{L_{i1j}}, P_{L_{i2j}}, P_{L_{i3j}}, \dots, P_{L_{(i_{\theta_1}-1)j}} \right\}. \quad (22)$$

If for $j\Delta\theta_2$, $\pi/2 < \Delta\theta_2 j < \Delta\theta_{w_{(i+1)} w_{(i+2)}}$:

$$\text{Plane}_{\text{Data}} = \left\{ P_{L_{i_{\theta_1} j}}, P_{L_{(i_{\theta_1}+1)j}}, P_{L_{(i_{\theta_1}+2)j}}, \dots, P_{L_{i_{m_1} j}} \right\},$$

$$\text{Wall}_{\text{Data}(i+1)} = \left\{ P_{L_{i1j}}, P_{L_{i2j}}, P_{L_{i3j}}, \dots, P_{L_{(i_{\theta_1}-1)j}} \right\}. \quad (23)$$

If for $j\Delta\theta_2$, $\Delta\theta_{w_{(i+1)} w_{(i+2)}} < \Delta\theta_2 j < \pi$:

$$\text{Plane}_{\text{Data}} = \left\{ P_{L_{i_{\theta_1} j}}, P_{L_{(i_{\theta_1}+1)j}}, P_{L_{(i_{\theta_1}+2)j}}, \dots, P_{L_{i_{m_1} j}} \right\},$$

$$\text{Wall}_{\text{Data}(i+2)} = \left\{ P_{L_{i1j}}, P_{L_{i2j}}, P_{L_{i3j}}, \dots, P_{L_{(i_{\theta_1}-1)j}} \right\}. \quad (24)$$

When the data segmentation above is finished, point clouds collected from a single laser after entire scanning process will be attached to three walls and one horizontal plane, ceiling, or floor.

4.3.3. Analysis of Point Cloud Segmentation in This Paper. As for the point cloud measured by the four lasers in the point cloud data, each laser contains four planes, including the point cloud data of three indoor walls and one plane (ceiling or floor). And the main idea of the above two algorithms is to segment the four planes of each one laser-scanning point cloud and then combine all the segmentation results from each laser to finally realize the segmentation of

the point cloud of the six planes in the whole room. Both algorithms use the different scanning path's characteristics of TLS in the hexahedron-type room. On-boundary segmentation uses edge features of indoor space, so two rounds of segmentation are required for point cloud data segmentation of single laser measurement data. One turn is for the edge feature of the intersection line between wall and plane, and the second turn is for the edge feature of the intersection line between wall and wall. On-angular-distance segmentation algorithm uses the angle features in space to segment point clouds. On the premise of knowing the size of indoor rooms, the angle features are used to realize the presegmentation of all point clouds on the walls. Thus, point cloud segmentation of four planes can be realized only through a cycle of data traversal. Therefore, the time complexity of on-angular-distance segmentation algorithm is lower.

To better understand the data process of the two algorithms, the principle of two algorithms can be understood through figure (see Figure 14). All point cloud can be regarded as a array in n_2 rows and n_1 columns. Due to the execution of "one-step process 2" for n_2 times, the arrays are combined with the n_2 son-arrays. The son-array which size of $1 \times n_1$ represents the point cloud scanned in "Procedure 1." In the point cloud segmentation scenario in this paper, the key of point cloud segmentation is to find the "cut-off point" for point cloud segmentation (the red areas of the picture represent the "cut-off points"). Although the on-angular-distance segmentation algorithm is better than the on-boundary segmentation in time complexity, the on-angular-distance segmentation algorithm needs to know get indoor room size, and the centre of TLS cannot be completely placed in the middle of the room during scanning, so the segmentation accuracy will be affected. On-boundary segmentation algorithm can segment point cloud without indoor house size. For regular hexahedral rooms, ideal point cloud segmentation can be achieved, but for indoor rooms with no obvious "edge features," the segmentation accuracy will be affected. Therefore, the advantages and disadvantages of the two algorithms should be analysed through segmentation experiments in actual point cloud in reality.

4.4. Plane Fitting Algorithm for Indoor Point Clouds

4.4.1. Rotation Transformation in Point Cloud Fitting. After the segmentation, the fitting of point clouds is launched. Higher accuracy of algorithm for fitting means higher accuracy of plane equation and higher accuracy of measuring results. However, during measuring, supervenient random error and assembly error of mechanized equipment will lead to a degree of error of final measuring data. Referring to pertinent literature, this paper adopts RANSAC-TLS algorithm for fitting 3D planes. In the majority of plane fitting with 3D point clouds, Z-axis is mostly set as the dependent variable of least squares fitting, which will result in that point clouds parallel to the XOY plane have priority to get fitting, and therefore, relatively great error may come out.

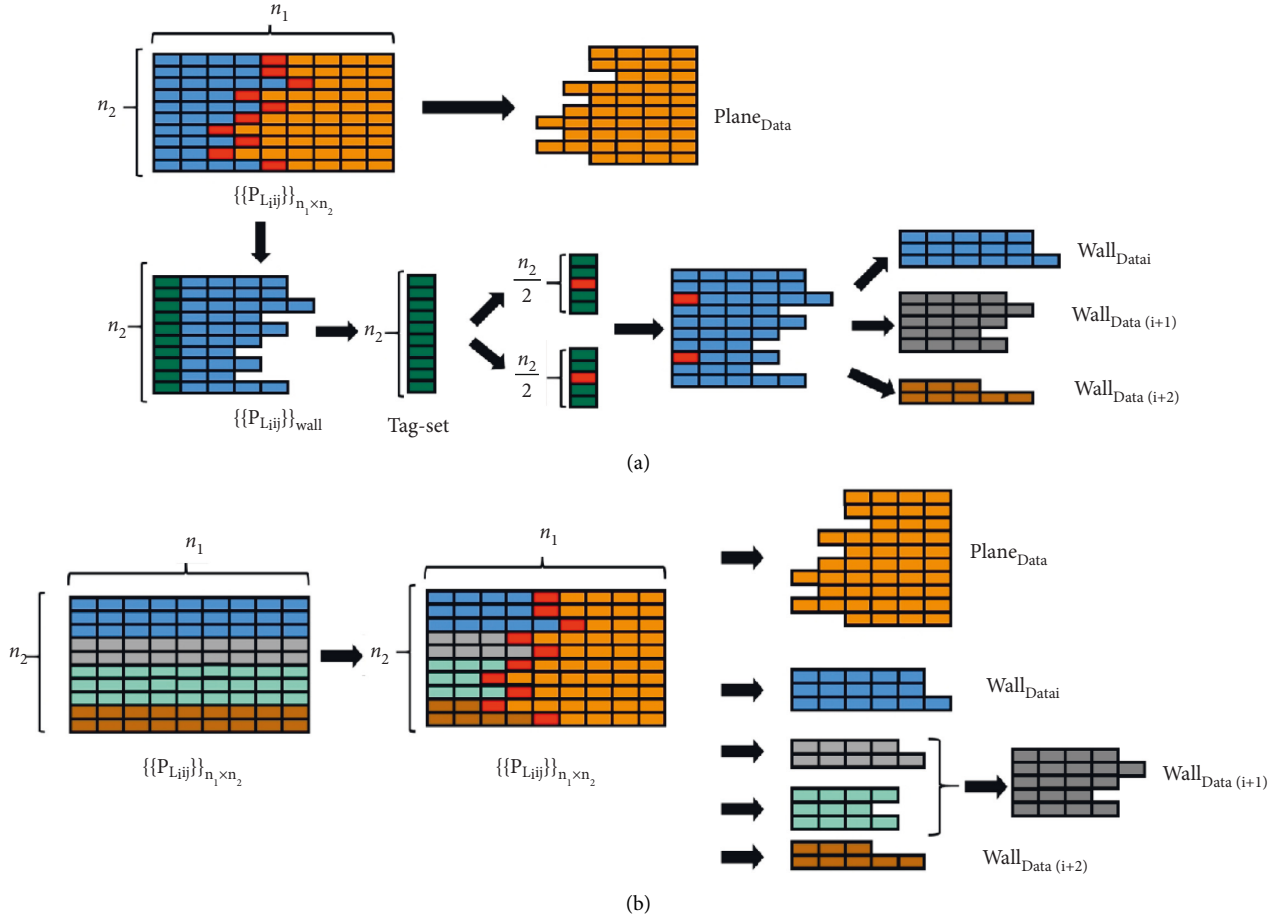


FIGURE 14: The diagram of point cloud segmentation in all. (a) On-boundary segmentation algorithm. (b) On-angular-distance segmentation algorithm.

$$P_{si} = (x_{si}, y_{si}, z_{si})^T. \quad (25)$$

When the point cloud cluster P_{si} rotates α_x degree around the x -axis, its rotation matrix is as follows:

$$rot_x = \begin{bmatrix} 1 & 0 & 0 \\ 0 & \cos \alpha_x & -\sin \alpha_x \\ 0 & \sin \alpha_x & \cos \alpha_x \end{bmatrix}. \quad (26)$$

The point cloud cluster after spatial transformation is P_{sxi} :

$$P_{sxi} = rot_x \times P_{si}. \quad (27)$$

When the point cloud cluster P_{si} rotates α_y degree around the y -axis, its rotation matrix is as follows:

$$rot_y = \begin{bmatrix} \cos \alpha_y & 0 & \sin \alpha_y \\ 0 & 1 & 0 \\ -\sin \alpha_y & 0 & \cos \alpha_y \end{bmatrix}. \quad (28)$$

The point cloud cluster after spatial transformation is P_{sxi} :

$$P_{syi} = rot_y \times P_{si}. \quad (29)$$

4.4.2. Modified RANSAC-TLS Algorithm for Fitting Based on Spatial Transformation

(1) *Total Least Squares*. Total least squares are a kind of algorithm for fitting that does not exclude interference factors in regression matrix during calculation. The basic principle of it is as follows:

The equation represents a surface

$$z = a_i x + b_i y + c_i. \quad (30)$$

Point cloud on the surface is present in the dataset $\{(x_i, y_i, z_i), i = 1, 2, \dots, n_i\}$, considering that there are errors on three directions of x, y, z and v_x, v_y, v_z are, respectively, three correction factors on x, y, z , and the equation of the surface above may be changed into:

$$z + v_z = a_i(x + v_x) + b_i(y + v_y). \quad (31)$$

It can be transformed as

$$(A + E_A)X = L + E_L,$$

$$A = \begin{bmatrix} x_1 & y_1 & 1 \\ x_2 & y_2 & 1 \\ \vdots & \vdots & \vdots \\ x_{ni} & y_{ni} & 1 \end{bmatrix},$$

$$E_A = \begin{bmatrix} v_{x_1} & v_{y_1} & 1 \\ v_{x_2} & v_{y_2} & 1 \\ \vdots & \vdots & \vdots \\ v_{x_{ni}} & v_{y_{ni}} & 1 \end{bmatrix},$$

$$X = \begin{bmatrix} a_i \\ b_i \\ c_i \end{bmatrix}, \quad (32)$$

$$L = \begin{bmatrix} z_1 \\ z_2 \\ \vdots \\ z_{ni} \end{bmatrix},$$

$$E_L = \begin{bmatrix} z_1 \\ z_2 \\ \vdots \\ z_{ni} \end{bmatrix}.$$

Generally, singular value decomposition of matrix (SVD) is used to solve the following equation:

$$[A \ L] = \begin{bmatrix} U_1 & U_2 \\ m+1 & n-m-1 \end{bmatrix},$$

$$\begin{bmatrix} \Sigma \\ 0 \end{bmatrix} V^T = U_1 \Sigma V^T,$$

$$V^T = \begin{bmatrix} V_{11} & V_{12} \\ V_{21} & V_{21} \\ m & 1 \end{bmatrix}, \quad (33)$$

$$U_1 = [U_{11} \ U_{12}],$$

$$\Sigma = \begin{bmatrix} \Sigma_1 & 0 \\ 0 & \Sigma_2 \\ m & 1 \end{bmatrix},$$

$$X = -V_{12}V_{22}^{-1}.$$

(2) *The Procedures of RANSAC-TLS Algorithm Based on Spatial Transformation.* First, point clouds on walls will be spatially transformed to become nearly parallel to plane XOY. Then, the RANSAC algorithm continuously removes the abnormal point clouds, and thus, the point clouds left will contain a relatively small quantity of abnormal point clouds. Finally, TLS will be used for fitting. The complete procedures of TLS are shown below:

- (1) Identifying the surface where point cloud P_{si} is and implementing spatial transformation on it according

to $P_{sxi} = rot_x \times P_{si}$ or $P_{syi} = rot_y \times P_{si}$, also $P_{si} = P_{sxi}$ or $P_{si} = P_{syi}$.

- (2) Selecting randomly three processed point clouds that are not on any common line and solving the equation of the three points: $z = a_i x + b_i y + c_i$.

- (3) Calculating the distance from every point cloud to the plane $z = a_i x + b_i y + c_i$ in the following formula:

$$d_i = \frac{|a_i x_i + b_i y_i + c_i - z_i|}{\sqrt{(a_i)^2 + (b_i)^2 + 1}}. \quad (34)$$

- (4) Calculating the standard deviation σ from point clouds to the plane d_i in the formula:

$$\sigma = \sqrt{\frac{\sum_{i=1}^n (d_i - \bar{d})^2}{n-1}}. \quad (35)$$

In the formula above, $\bar{d} = 1/n \sum_{i=1}^n d_i$, and thresholding $t = 2\sigma$. If $d_i > t$, then the point is identified as null point ready to be deleted; otherwise, the point is efficient point to be retained and the amount of efficient points will be totaled to M_i .

- (5) Repeating the procedures above k times and identifying the model with most efficient points: $M_f = \max\{M_i\}$.
- (6) Adopting TLS to conduct point clouds fitting of surfaces and obtaining the parameters of plane equations.

5. Experimental Verification and Discussion

5.1. Experiment Preparation

5.1.1. *Preparation of TLS in This Paper.* In order to verify the feasibility of the novel TLS and data processing system, we conducted scanning and processing in several rooms ready-to-move-in in a room shape that basically conforms with a hexahedron (see Figure 15(a)).

We implemented 3D scanning to collect data of the room on the novel self-adaptation TLS equipment; as for software system for laser scanning, we designed and developed two software systems: one for data collecting and the another for point cloud processing. All data collection was carried out on the equipment (see Figure 15(c)), and then, the data were transferred to a cloud server through which the scanning data were downloaded into a computer terminal to implement processing. In this paper, we temporarily adopted TCP/IP on a local area network to transfer the data for the sake of short-term experimental stage.

When the TLS machine was appropriately located, we clicked on the "To Scan" to start 3D scanning of the entire room. After it finished, scanning points were transferred to computer where we proposed two novel point cloud segmentation algorithms: one based on edges of interior surfaces and one based on angle range. On data-processing interface, the process of the data point processing was visualized and the interior quantities of room were obtained by data processing (see Figure 15(b)).

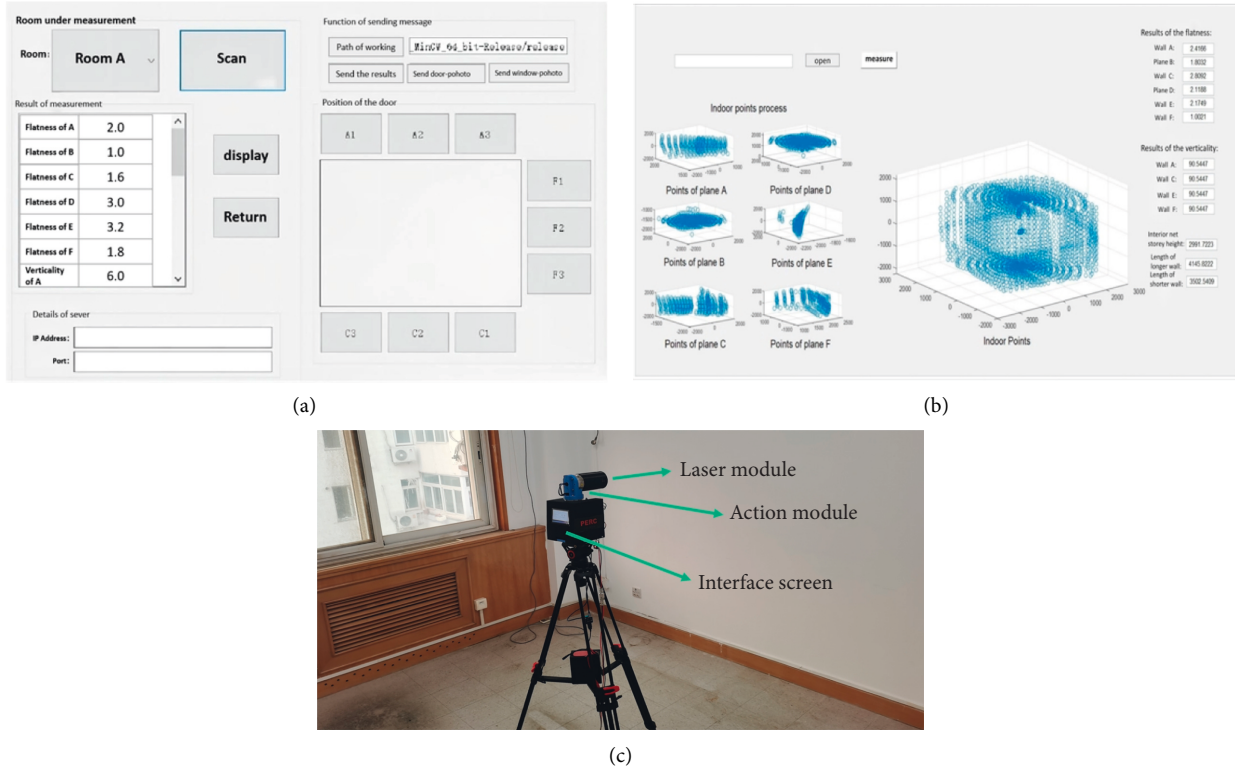


FIGURE 15: The platform of indoor measurement. (a) Interface of TLS. (b) Interface of PC. (c) TLS designed in this article.

5.1.2. *Experiment Process of Data Analysis.* Afterwards, the collected data will be processed on computer and the entire processing procedures are displayed in Figure 16. We collected indoor 3D point cloud data with the multilaser module on the self-adaptation novel TLS equipment, but there was a possibility for laser beam to hit outside the room or on some light-reflecting objects causing high measuring error of data and high error of the point clouds corresponding to the measured data, which were called noisy points. Hence, we needed the filter mentioned in the paper to filter out the noisy points and retain point clouds applicable to indoor point cloud processing. Then, retained indoor point clouds were segmented by the point cloud segmentation algorithms for point clouds. The segmented clusters of point clouds were fitted into different surfaces. The equations of fitted surfaces will be used in the analysis of the measuring accuracy of this measuring system with a traditional manual laser-ranging method.

5.1.3. *The Evaluation for Segmentation Algorithms for Indoor Point Clouds.* To evaluate the measuring accuracy of two kinds of segmentation algorithms proposed in this paper for indoor point clouds and analyse the merits and defects of the two algorithms, we referred to and selected the precision, recall, and F1 index to perform as the evaluating standard [32]. The equation of them is as follows:

$$\left\{ \begin{array}{l} \text{precision} = \frac{N_t}{N_t + N_o}, \\ \text{recall} = \frac{N_t}{N_t + N_c}, \\ F_1 = \frac{2 \times \text{recall} \times \text{precision}}{\text{precision} + \text{recall}}. \end{array} \right. \quad (36)$$

The N_p , N_o , and N_e , respectively, represented the numbers of relatively accurately segmented point clouds, omissive-in-segmenting point clouds, and wrongly segmented point clouds.

5.1.4. *The Verification for Fitting Accuracy of Indoor Point Clouds.* Once the data processing was finished, we started verifying the fitting accuracy of segmented point clouds of surfaces. The verifying method was proposed by making use of calibrating method for indoor measuring and also the characteristics of measured objectives—indoor rooms.

(1) *Calibration for Indoor Measurement.* We calibrated the measurement in manual way and the calibrated objective is the net-length of the room. Specifically, we measured the net-length from the laser range finder in hand to the laser point hits on a relatively smooth surface and repeated the measurement on multipoints many times. Afterwards, we

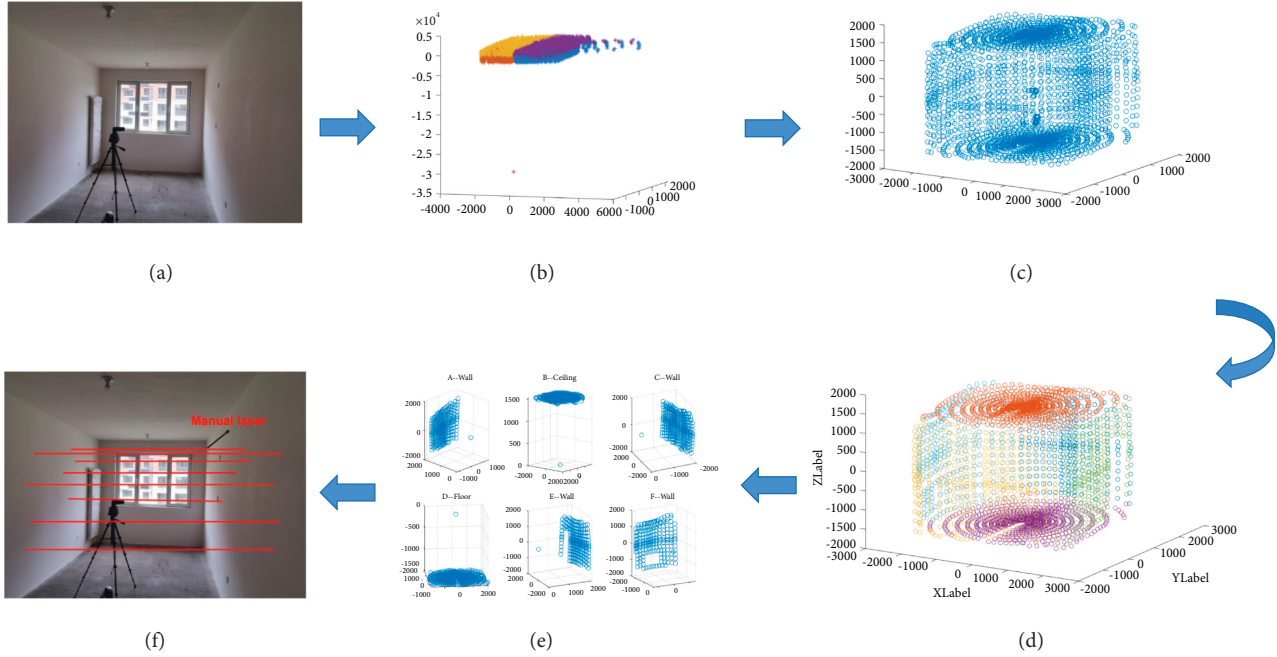


FIGURE 16: The flow chart of the point cloud processing in indoor measurement experiment. (a) Indoor TLS measurement. (b) Indoor point clouds of laser scanning. (c) Indoor point clouds of filtering. (d) Indoor point clouds of structural segmentation. (e) Indoor point clouds of fitting. (f) Manual measurement for precision checking.

calculated the average value of all measuring results. Measuring value in every time was marked as L_{mi} ($i = 1 \dots n$).

The standard value for calibration is as follows:

$$L_{ms} = \frac{\sum_{i=1}^n L_{mi}}{n}. \quad (37)$$

(2) *The Evaluation for the Fitting Accuracy of Point Clouds.* The plane equations of two planes obtained by fitting algorithm were as follows: $A_s x + B_s y + C_s z + D_s = 0$ and $A_j x + B_j y + C_j z + D_j = 0$.

The vertical distances of two plane equations to the origin, also the pose of the TLS equipment, were marked, respectively, as d_s and d_j , and their values can be calculated in the formulae for distance presented below.

$$\begin{cases} d_s = \frac{|D_s|}{\sqrt{(A_s)^2 + (B_s)^2 + (C_s)^2}}, \\ d_j = \frac{|D_j|}{\sqrt{(A_j)^2 + (B_j)^2 + (C_j)^2}}. \end{cases} \quad (38)$$

The net-length obtained from the equipment was as follows:

$$L_{TLS} = d_s + d_j. \quad (39)$$

Comparing the L_{TLS} with the standard value for calibration L_{ms} , the difference value can reflect the measuring accuracy.

5.2. Experiment Result and Discussion

(1) *The Analysis of Effectiveness of 3D Scanning.* The results of actual indoor 3D scanning data collected by the novel self-adaptation TLS equipment might basically reflect indoor constructional features, and the general configuration of windows and door in the real room was presented by visualizing 3D point clouds data (see Figure 17).

(2) *The Result of Point Cloud Segmentation.* As shown in Figure 18, for point clouds from hexahedral room with clear boundaries between surfaces, “on-boundary segmentation algorithm” will perform relatively effective segmentation but for that from rooms without clear boundaries of surfaces, and the segmentation results of “on-boundary segmentation algorithm” are not close to 6 indoor surfaces. The unclear boundaries of surfaces are shown in these two forms: (1) carvings made between ceiling and walls, and (2) relatively big internal and external corner existing on the edge zones of surfaces. However, “on-angular-distance segmentation algorithm” will be able to perform normal segmentation under these two kinds of conditions and it is noticeable that known room indoor sizes are the premise of performing high-accuracy segmentation.

We have implemented data scanning and collecting of the two kinds of rooms in different conditions and evaluation of segmentation accuracy of two types of segmentation algorithms mentioned in this paper (shown in Table 2). On house type of room 1, the performance of two kinds of segmentation algorithms is ideal, with the F1 index of point cloud clusters from “on-boundary segmentation algorithm” up to highest value of 0.9663 and the down to 0.7692 and the F1 index from “on-angular-distance segmentation algorithm” ranging from 0.6866

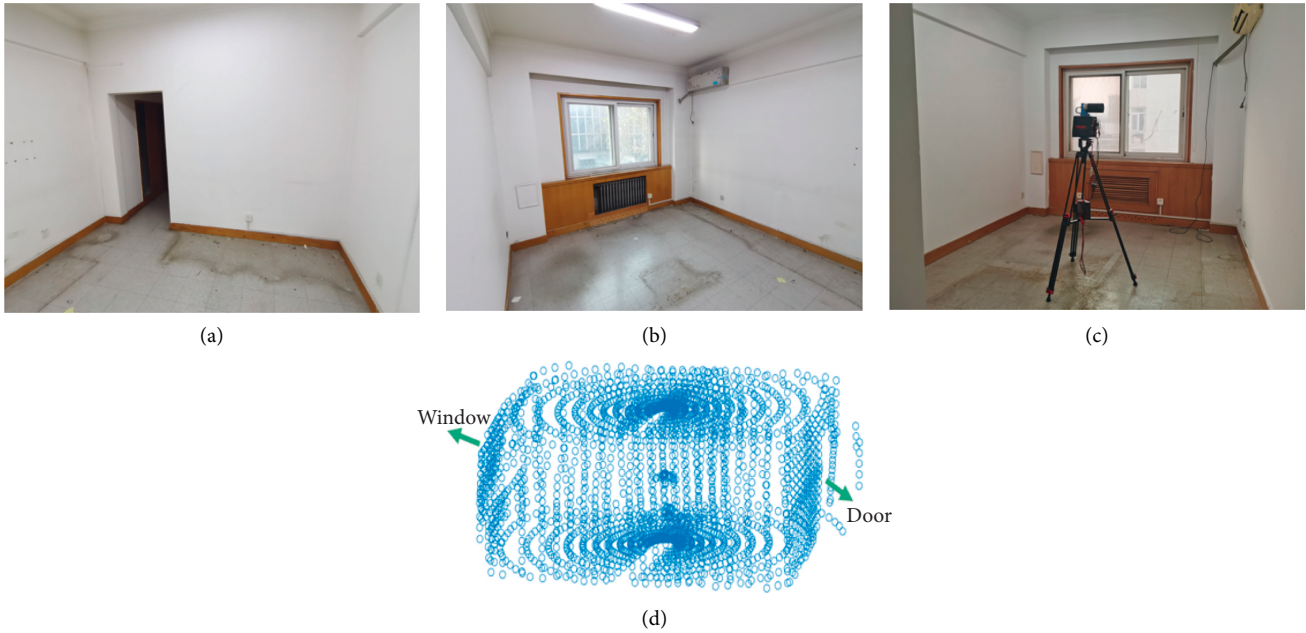


FIGURE 17: Actual room and point cloud of scanning. (a) Actual room in view 1. (b) Actual room in view 2. (c) Actual experiment in actual room. (d) Scanning point cloud in actual room.

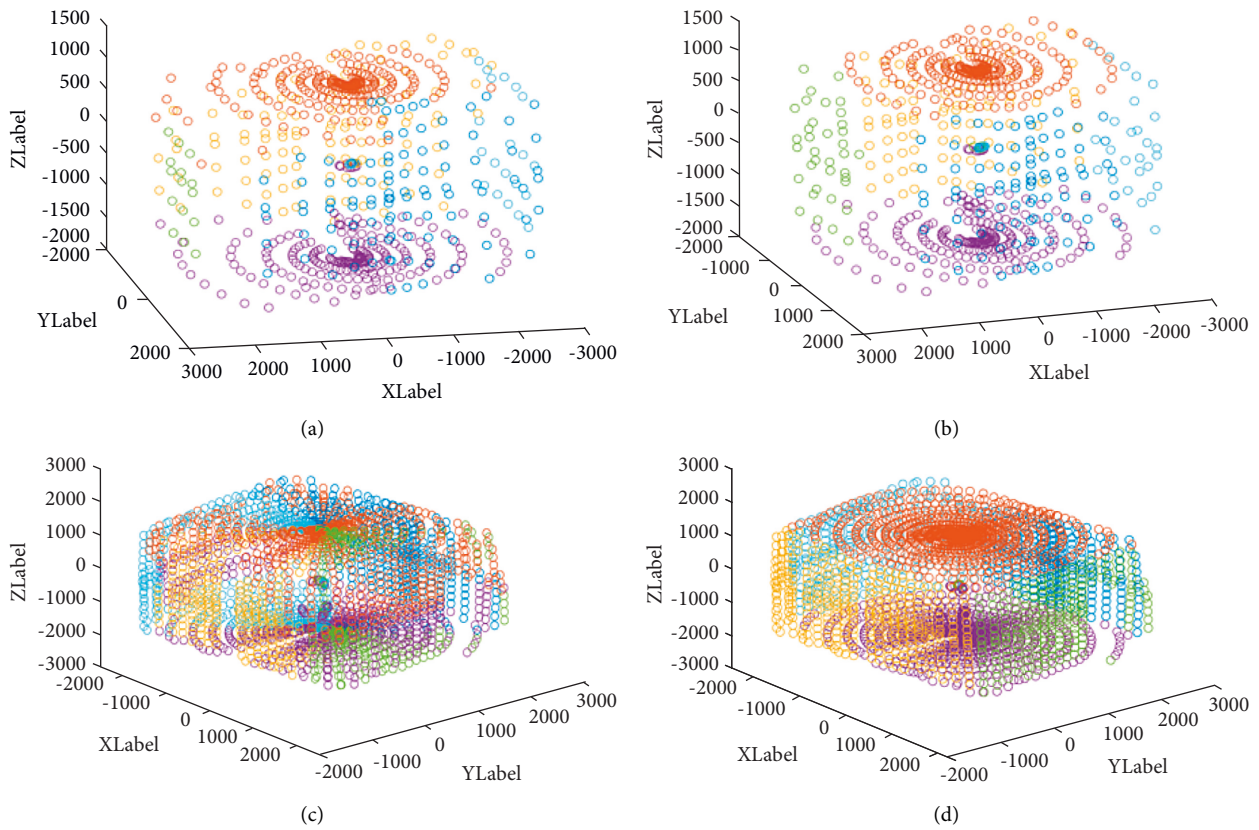


FIGURE 18: The result of the point cloud segmentation. (a) On-boundary segmentation in room 1. (b) On-angular-distance segmentation in room 1. (c) On-boundary segmentation in room 2. (d) On-angular distance segmentation in room 2.

to 0.9789. As for house type of room 2, the segmentation accuracy of “on-angular-distance segmentation algorithm” is higher than that in another. Highest F1 index of point cloud

clusters from “on-boundary-segmentation algorithm” is 0.7713 and the lowest one is 0.2969, while the F1 index from the another segmentation algorithm has highest value of 0.9781 and

TABLE 2: Evaluation of the point cloud segmentation.

Type of the room	Segmentation algorithm	Index	Number of point cloud cluster					
			1	2	3	4	5	6
Room 1	On-boundary segmentation	Numbers	94	228	105	215	20	30
		Precision	0.9362	0.9561	0.9238	0.9805	0.8824	0.9000
		Recall	0.9671	0.9689	0.9604	0.9526	0.6818	0.7500
	On-angular-distance segmentation	F_1	0.9514	0.9625	0.9417	0.9663	0.7692	0.8182
		Numbers	88	227	105	214	27	31
		Precision	0.9545	0.9824	0.8762	0.9766	0.7407	0.7419
		Recall	0.9333	0.9696	0.9388	0.9812	0.9091	0.6389
		F_1	0.9438	0.9759	0.9064	0.9789	0.8163	0.6866
Room 2	On-boundary segmentation	Numbers	392	649	265	705	247	441
		Precision	0.6582	0.6336	0.8302	0.9062	0.3644	0.2063
		Recall	0.9314	0.50141	0.9016	0.4628	0.4348	0.5291
	On-angular-distance segmentation	F_1	0.7713	0.5598	0.8644	0.6127	0.3965	0.2969
		Numbers	278	777	362	800	221	261
		Precision	0.9389	0.9781	0.8785	0.9750	0.9638	0.7510
		Recall	0.7957	0.9596	0.9845	0.9811	0.8987	0.8167
		F_1	0.8614	0.9688	0.9285	0.9781	0.9301	0.7824

lowest one of 0.7824. From the perspective of data, we can draw a conclusion that these two kinds of segmentation algorithms are both able to attain relatively high-accuracy segmentation for indoor point clouds and the accuracy of segmentation is lower when the segmented objective is a lesser order of magnitudes of point cloud clusters.

Apart from that, viewing for the segmentation accuracy of room 2, whereas the distinction of surfaces in the house type as room 2 is less significant relative to that of room 1, the particular point clouds used for “on-boundary segmentation” are not easy to identify, and hence, the segmentation accuracy is not high. On the other hand, the accuracy of two kinds of segmentation algorithms for two rooms is basically close, attributing to the oneness of determinant for the segmentation accuracy of “on-angular-distance segmentation algorithm”—the accuracy degree of distance from equipment to every surfaces in a room.

Hence, the key to enhance the accuracy of segmentation is to ensure the room size and type as near to a standard hexahedron as possible and also the normative location of the TLS equipment at the centre of a room.

(3) *The Accuracy of Point Cloud Fitting.* After finishing the point cloud segmentation, this paper selects the segmented point cloud clusters of two planes with symmetrical distribution for plane fitting and plane distance calculation. And we calculated the actual distance result through the manual measurement, which was carried out by the method proposed above. Referring to relevant literature, in the fitting process, this paper selects different plane fitting algorithms, including TLS, LS, WTLS-D, RANSAC-LS, and the improved RANSAC-TLS proposed in this paper.

In the fitting experiment, we divided the segmented point cloud clusters into three categories: class 1 point cloud clusters, class 2 point cloud clusters and class 3 point cloud clusters. Among them, class 1 point cloud clusters were mainly the point cloud clusters distributed on the two opposite walls with the largest area of the blank part on the

indoor surface; class 2 point cloud clusters were the point cloud clusters on the floor and ceiling; and class 3 point cloud clusters referred to the point cloud clusters on the wall with windows and opposite to the wall. We selected five house types of rooms for data scanning and point cloud segmentation, and three kinds of point cloud clusters were extracted for fitting accuracy experiment. The experimental results are shown in the Figure 19.

It can be seen from the figure that among class 1, class 2, and class 3 point cloud clusters, RANSAC-TLS algorithm is the closest to the results of manual measurement. The second is RANSAC-LS and WTLS-D algorithm. LS and TLS algorithm performed worst in fitting, and the changing trend of the two algorithms is similar in the calculation results of different rooms. Because there were some noise points of information in the whole segmented point cloud cluster, these noise points are composed of random error in the scanning process and systematic error of the equipment. Moreover, in the process of point cloud segmentation, because the segmented point cloud clusters are sparse point cloud clusters, and not all of the point cloud clusters are ideal point clouds in the flat wall area; on the contrary, there are often some outliers in the point cloud clusters, which become noise points in the sparse point cloud clusters and affect the fitting accuracy evaluation results.

According to the measurement results, LS and TLS do not filter all point cloud data in the fitting process, so these two algorithms are easy to introduce some noise data into the fitting process. Although WTLS-D algorithm also performed iterative fitting based on the distance to the TLS plane as the weight, its initial fitting plane was still the fitting result of TLS. Therefore, in the fitting process, although its fitting accuracy was improved, its robustness was relatively poor. Both RANSAC-LS and RANSAC-TLS belong to combined algorithms, which get the advantages of RANSAC algorithm. The ideal point cloud region of plane fitting was found by calling out a reasonable threshold. From the results, compared with RANSAC-LS, RANSAC-TLS

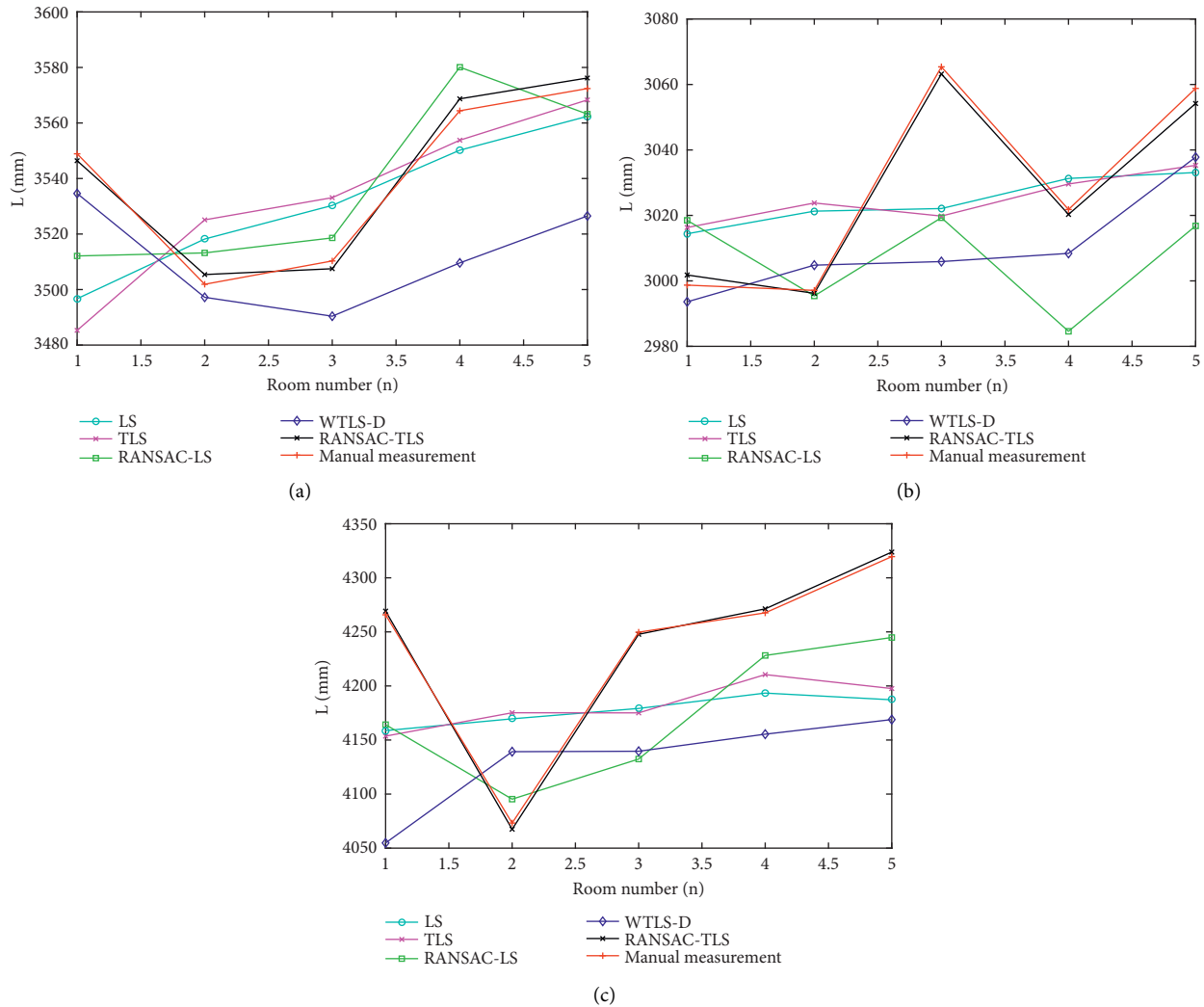


FIGURE 19: The result of the point cloud fitting and manual measurement. (a) Result of class 1 point cloud. (b) Result of class 2 point cloud. (c) Result of class 3 point cloud.

better optimized the fitting weights of all point clouds in the filtered point cloud data, and finally performed better in the fitting results. For class 1 point cloud, it could be seen that there were relatively few noise points in its point cloud cluster, so all fitting algorithms were relatively stable in the measurement results. However, complex outliers would appear in the data scanning of class 2 and class 3 point cloud clusters. For example, the point cloud of objects such as lampshade often appeared in the ceiling data in class 2 point cloud clusters. In the three kinds of point cloud clusters, due to the measurement target of window, there would be more complex point cloud clusters. For the point cloud fitting algorithm without prescreening in the fitting process, the calculation results based on the fitting plane equation would have a large deviation from the actual measurement results.

Thus, in the fitting process, RANSAC can screen out noise and outliers and improve the fitting accuracy. From the overall fitting results, RANSAC-TLS algorithm performs best in fitting accuracy.

(4) *Analysis of Scanning Parameters Threshold in Actual Measurement.* To test measurement accuracy and efficiency of the proposed planning-scanning method in real indoor condition, we conducted one measurement experiment with the novel TLS equipment in a room, in shape of a hexahedron, ready to move in, in size of 4250 mm × 3510 mm × 3065 mm. According to the planning-scanning method proposed in Chapter 3, the relevant planning parameters in this house shape include $D_0 = 142$ mm, $L_b = 4250$ mm, $L_c = 3510$ mm, $s_{max} = 330$ mm, $T_d = 0.5$ s, and $T_s = 1$ s.

For the planning model of indoor scanning, s_{max} is a reference value, and value s_0 determines the distributing density of the entire laser scanning point cloud data. To make TA a relatively small value, which is an expectation, s_{max} is usually taken from s_0 , and k is taken as large as possible. In this experiment, for value taking, we set different s_0 values for actual data collecting. Besides, we obtained segmented point cloud clusters and the point-

TABLE 3: Experimental parameters in different schemes.

	T_A (min)	S_0 (mm)	θ_c (°)	k	θ_c (°)	$\Delta\theta_2$ (°)	File size (kB)
Manual measurement	25						
Scheme 1	13	330	4.75	2	5	10	26
Scheme 2	26	330	4.75	1	5	5	56
Scheme 3	10	400	5.87	1.67	6	10	20
Scheme 4	15.25	200	2.78	3.33	3	10	30
Scheme 5	4.75	630	9.89	1	10	10	7

TABLE 4: Result of actual measurement with different schemes.

(mm)	Wall 1		Wall 2		Wall 3		Wall 4		mF.E	mV.E
	F.R	V.R	F.R	V.R	F.R	V.R	F.R	V.R		
Manual measurement	3.33	7	3	2.26	3	2	2.5	4.5		
Scheme 1	2.528	6.32	2.716	5.67	2.134	6.18	1.182	6.94	0.82	2.68
Scheme 2	3.47	5.32	4.22	1.24	4.13	1.71	2.0	6.33	0.75	1.21
Scheme 3	4.247	6.34	4.34	5.79	4.58	6.126	2.513	6.87	0.96	2.67
Scheme 4	3.503	6.38	4.25	5.78	3.86	5.71	1.683	6.44	0.78	2.45
Scheme 5	2.55	2.32	3.857	1.34	2.09	13.6	2.11	6.45	1.78	5.79

TABLE 5: Comparison of the device parameters.

Device parameters	FARO focus M70	Novel TLS
Measurement accuracy	±1 mm	±1 mm
Laser module type	LIDAR module	Point laser module
Range of distance measurement	0.6 m–70 m	0.3 m–10 m
Measurement speed	488000 points/s	4 points/s
Vertical field of scanning	305°	360°
Horizontal field of scanning	360°	360°
External dimensions (mm)	240 * 200 * 100	350 * 300 * 300
The characteristics of the scan	The dense point cloud is used to reconstruct the 3D space and completely simulate the measured indoor real quantity	Measure the indoor real quantity with spare point cloud of point cloud process

TABLE 6: Comparison of the two devices for actual measurement.

Device name	Scanning time (min)	mF.E (mm)	File size	Equipment cost (\$)
FARO focus M70	4	0.7 ^[21]	7.68 GB	90,000
Novel TLS 1	5	1.8	7 kB	7,000
Novel TLS 2	13	0.8	26 kB	7,000

cloud-cluster-plane equation based on the proposed point-cloud-processing algorithm.

Referring to the calculation method presented in the relevant literature [33], the flatness and verticality of four indoor walls of the measured room are calculated with different scanning parameter. In addition, we obtained the same two indexes by manual measurement with guiding rule. Based on the above operation, the mean error of flatness (mF.E) and mean error of verticality (mV.E) can be achieved by first attaining errors between manually measured values and variable values coming from the novel TLS equipment with varying scanning parameters.

Next, the calculation is executed in method proposed in this paper alike with changing scanning parameter, and the

results of the actual manual measurement, respectively, find the error of the measurement value and manual measurement value of the equipment based on different scanning parameters, and calculate the mF.E of the wall and the mV.E of the wall.

Five groups of real quantities of measured indoor walls were taken from the entire experiment (see Table 3). As shown in the below table, S_0 ranges from 200, 330, 400, and 630. When S_0 and k are both in a relatively-low value, T_A will reach an excessively large value. In this case, $\Delta\theta_2$ was once set at 10° by controlling the value of k . Additionally, with s_0 in value of 330 and meanwhile $\Delta\theta_2$ at 5°, a scanning was executed for contrasting (shown in Table 4) presents the specific experiment results.

From the calculation results with different parameters, it should be known that although the scanning scheme 2 takes the

longest time, the measurement results have the smallest mean error by being compared with manual measurement results. The scanning scheme 5 takes the shortest time, but the measurement mean error is the largest in the same comparison pattern. Walls 3 and 4 are two walls further away from the novel TLS equipment than the other two, corresponding to point cloud clusters 5 and 6. Associating with the point cloud segmentation results, it can be concluded that point clouds distributed on the two walls are less so that the wall point cloud data are less and the measurement error emerges greater, which is less, and the measurement error is greater. Because of lower mV.E value in scheme 2, it might be true that minimizing $\Delta\theta_2$ is more efficient in enhancing measurement accuracy. However, scheme 2 has one flaw that the time consumption of scanning in this scheme is even larger than traditional manual measurement method.

5.3. Comparison Result between the Novel TLS and the Existing TLS

(1) *Comparison of the Device Parameters.* Most existing TLS adopted in indoor measurement is nothing more than FARO Focus 3D laser scanner. In Table 5, the parameters of the two TLS devices are compared, and the existing TLS devices have higher efficiency and density in environment-sensing data collection. However, the existing TLS equipment and the novel TLS equipment can both achieve ranging accuracy ranging within ± 1 mm. In another word, in the perspective of scanning range, the mechanical structure of the novel TLS equipment proposed in this paper has no scanning blind area.

(2) *Comparison of the Actual Measurement Result.* In order to verify the further application and practical potential of the novel TLS equipment in indoor actual measurement, we compare the measurement accuracy, efficiency, and cost of FARO focus [21] and novel TLS in similar experimental conditions, taking the mF.E results of flatness in the indoor slab measurement [21] as accuracy-evaluating standard. Next, contrasting FARO equipment and the novel TLS equipment in two aspects are presented in Table 6: scanning time and amount of point cloud data in actual measurement.

As seen in Table 6, in scanning time consumption, the scanning scheme 1 of the novel TLS equipment proposed in this paper is 1 minute slower than FARO. The measurement accuracy in scanning scheme 2 is 0.8 mm, near to FARO. However, the cost of novel TLS equipment is much lower than FARO. Besides, in the aspect of file size of scanning data, the novel TLS equipment features lower cost of data processing due to its smaller size of collected scanning data than existing TLS equipment.

6. Conclusion and Future Research

It can be concluded that the novel TLS presented in this paper is able to achieve self-adaptation scanning in indoor condition. As for P4S, this paper presents a “scanning method by process” to realize planning for scanning of an indoor space of a room. In view of continuous changes of point clouds poses in one-step

process in “measurement by process,” the segmentation methods mentioned in this paper not only make use of point clouds extracted from TLS, which is a kind of discrete data, but also make use of the poses of every laser scanning points. Finally, the actual measurement tests display that the “on-angular-distance segmentation algorithm” is of higher robustness than “on-boundary segmentation algorithm” in actual measurement. However, if the measured room is near to a regular hexahedron, the accuracy of the two segmentation algorithm is close. In terms of fitting of point clouds, this paper presents a modified plane fitting algorithm based on the point cloud distribution characteristics in a hexahedral room and it is proved that the modified plane fitting algorithm can achieve millimetre-level accuracy. Accuracy and efficiency of the novel TLS may be tested by analysing measured quantities drawn from an actual measurement experiment with a threshold of equipment parameters. Furthermore, for testing accuracy and efficiency, this paper introduces a series of measurement results of an existing TLS equipment, FARO, attained in basically the same conditions to compare with that of the novel TLS equipment proposed in this paper, with costs of the two pieces of equipment being compared too. In this way, the accuracy, efficiency, cost and potential, and future application of the proposed novel TLS equipment based on sparse point clouds are preliminarily tested.

Although the self-adaptation TLS has merits of self-planning, low-cost, and high-efficiency computing, there is an abundance of optimisation and upgrading to fulfil: 1. creating structural parameter calibration methods because several parameters are introduced in the DH modelling, which brings some systematic errors into the result, requiring an appropriate calibration scheme to reduce the systematic error; 2. upgrading segmentation algorithm based on structural characteristics of irregular room. This paper achieves segmentation of point clouds from a regular hexahedral room, but if the room structure is more complicated, the robustness of the segmentation algorithm is apt to decline; 3. by implementing semantic segmentation of the indoor information based on this kind of lightweight dataset presented in this paper, this paper has just researched data features of wall surfaces but not covered semantic segmentation for indoor 3D data or segmentation for details, such as those of doors and windows, and internal and external corners. Therefore, our team will continue relevant researches and tests in the future.

Data Availability

The data used to support the findings of this study are available from the corresponding author upon request.

Conflicts of Interest

The authors declare that they have no conflicts of interest regarding the publication of this paper.

Acknowledgments

This study was sponsored by the BUCEA Doctor Graduate Scientific Research Ability Improvement Project (DG2021015), Key Science and Technology Projects of China

(KZ202110016024), and BUCEA Master Graduate Scientific Research Ability Improvement Project (PG2022128).

References

- [1] I. Jeong, Y. Jang, J. Park, and Y. K. Cho, "Motion planning of mobile robots for autonomous navigation on uneven ground surfaces," *Journal of Computing in Civil Engineering*, vol. 35, no. 3, 2021.
- [2] R. K. Bharadwaj and B. G. D. Soto, "Task allocation and route planning for robotic service networks in indoor building environments," *Journal of Computing in Civil Engineering*, vol. 31, no. 5, Article ID 04017038, 2017.
- [3] J. Li, J. Wu, and J. Li, "Blockchain-based trust edge knowledge inference of multi-robot systems for collaborative tasks," *IEEE Communications Magazine*, vol. 59, no. 7, pp. 94–100, 2021.
- [4] B. Nva, E. Bpc, B. Gz, N. X. Hung, and P. Tran, "Digital design computing and modelling for 3-D concrete printing," *Automation in Construction*, vol. 123, 2020.
- [5] A. Zhu, P. Pauwels, and B. D. Vries, "Smart component-oriented method of construction robot coordination for prefabricated housing," *Automation in Construction*, vol. 129, 2021.
- [6] B. G. De Soto, I. Agusti-Juan, J. Hunhevcz, S. Joss, and K. Graser, "Productivity of digital fabrication in construction: cost and time analysis of a robotically built wall," *Automation in Construction*, vol. 92, pp. 297–311, 2018.
- [7] F. Xu, S. Dai, Q. Jiang, and X. Wang, "Developing a climbing robot for repairing cables of cable-stayed bridges," *Automation in Construction*, vol. 129, no. 6, Article ID 103807, 2021.
- [8] S. Wang, H. Zhou, Z. Zhang, X. Zheng, and Y. Lu, "Robot floor-tiling control method based on finite-state machine and visual measurement in limited FOV," *Advances in Civil Engineering*, vol. 2021, Article ID 8372815, 16 pages, 2021.
- [9] A. Yl, B. Mh, and C. Hj, "Brain-computer interface for hands-free teleoperation of construction robots," *Automation in Construction*, vol. 123, 2020.
- [10] D. Wfabc, B. Lda, D. Pedl, H. Luo, H. Li, and C. Zhou, "Computer vision applications in construction safety assurance," *Automation in Construction*, vol. 110, 2019.
- [11] N. Narendrakrishnan, S. Asbjørn, K. Bhavatarini, A. B. Jakob, and N. Roberto, "Applying software design patterns to graph-modelled robotic workflows," *Automation in Construction*, vol. 132, ScienceDirect.
- [12] A. HJw, A. Ma, A. Ok, Z. Bhiri, M. Buck, and O. Kyjanek, "Flexible and transportable robotic timber construction platform – tim," *Automation in Construction*, vol. 120, 2021.
- [13] C. Chen, *Heterogeneous integration of BIM with low-cost indoor mobile laser scanning method for building fabric maintenance in China*, PhDAdvisor, 2019.
- [14] R. Chacón, C. P. Polo, and E. R. eal, "TLS measurements of initial imperfections of steel frames for structural analysis within BIM-enabled platforms," *Automation in Construction*, vol. 125, no. 6, 2021.
- [15] A. Guarnieri, N. Milan, and A. Vettore, "Monitoring of complex structure for structural control using terrestrial laser scanning (tls) and photogrammetry," *International Journal of Architectural Heritage*, vol. 7, no. 1, pp. 54–67, 2013.
- [16] N. Zikova, Z. Ziembiak, T. Olszowski, M. Bozym, and J. Rybak, "Elemental and microbiota content in indoor and outdoor air using recuperation unit filters," *Science of the Total Environment*, vol. 789, Article ID 147903, 2021.
- [17] A. Aryan, F. Bosche, and P. Tang, "Planning for terrestrial laser scanning in construction: a review," *Automation in Construction*, ScienceDirect, vol. 125, 2021.
- [18] B. Quintana, S. A. Prieto, A. Adán, and A. S. Vazquez, "Semantic scan planning for indoor structural elements of buildings," *Advanced Engineering Informatics*, vol. 30, no. 4, pp. 643–659, 2016.
- [19] Z. Cheng, V. S. Kalasapudi, and P. Tang, "Rapid data quality oriented laser scan planning for dynamic construction environments," *Advanced Engineering Informatics*, vol. 30, no. 2, pp. 218–232, 2016.
- [20] N. Puri, E. Valero, Y. Turkan, and F. Bosche, "Assessment of compliance of dimensional tolerances in concrete slabs using TLS data and the 2D continuous wavelet transform," *Automation in Construction*, vol. 94, pp. 62–72, 2018.
- [21] F. Bosché and E. Guenet, "Controlling slab flatness automatically using laser scanning and BIM," in *Proceedings of the 31st ISARC*, Sydney, Australia, January 2014.
- [22] F. Bosche, C. T. Haas, and B. Akinci, "Automated recognition of 3D CAD objects in site laser scans for project 3D status visualization and performance control," *Journal of Computing in Civil Engineering*, vol. 23, no. 6, 2009.
- [23] J. Guo, L. Yuan, and Q. Wang, "Time and cost analysis of geometric quality assessment of structural columns based on 3D terrestrial laser scanning," *Automation in Construction*, vol. 110, Article ID 103014, 2020.
- [24] Y. Zhang, C. Li, B. Guo, C. Guo, and S. Zhang, "KDD: a kernel density based descriptor for 3D point clouds," *Pattern Recognition*, vol. 111, no. 2, Article ID 107691, 2021.
- [25] M. Zine-El-Abidine, H. Dutagaci, G. Galopin, and D. Rousseau, "Assigning apples to individual trees in dense orchards using 3D colour point clouds," *Biosystems Engineering*, vol. 209, pp. 30–52, 2021.
- [26] C. Zhao, H. Guo, J. Lu, D. Yu, and Y. Lin, "A new approach for roof segmentation from airborne LiDAR point clouds," *Remote Sensing Letters*, vol. 12, no. 4, pp. 377–386, 2021.
- [27] C. Yin, B. Wang, J. Vincent et al., "Automated semantic segmentation of industrial point clouds using ResPoint-Net++[J]," *Automation in Construction*, vol. 130, Article ID 103874, 2021.
- [28] S. Park, S. Ju, S. Yoon, M. H. Nguyen, and J. Heo, "An efficient data structure approach for BIM-to-point-cloud change detection using modifiable nested octree," *Automation in Construction*, vol. 132, no. 9, Article ID 103922, 2021.
- [29] A. Mb, B. Kn, B. Jgm, M. H. F. Wilkinson, and J. G. Messchendorp, "An efficient attribute-space connected filter on graphs to reconstruct paths in point-clouds," *Pattern Recognition*, vol. 106, 2020.
- [30] Y. Duan, C. Yang, H. Chen, and W. Yan, "Low-complexity point cloud filtering for LiDAR by PCA-based dimension reduction," *Optics Communications*, 2020.
- [31] P. W. Birkeland and L. J. Westhoff, "Dimensional tolerances in a tall concrete building," *Journal of the American Concrete Institute*, pp. 600–607, 1971.
- [32] C. Zhang, K. Zhang, L. Ge, K. Zou, and S. Wang, "A method for organs classification and fruit counting on pomegranate trees based on multi-features fusion and support vector machine by 3D point cloud," *Scientia Horticulturae*, 2020.
- [33] Z. Zhang, H. Zhou, and S. Wang, "Research on global actual measurement of indoor surface flatness and verticality Based on sparse point cloud," *Journal of Physics: Conference Series*, vol. 2215, Article ID 012015, 2022.